Surfactant functionalized cobalt silica membranes – gas permeation and thin film positron annihilation lifetime spectroscopy characterisation

Gianni Olguin[1,2*], Christelle Yacou[1,3], J. Motuzas[1], Maik Butterling[4], Wilhelm A. Meulenberg[5], Simon Smart[1], João C. Diniz da Costa[1,6,7*]

Highlights

- PALS depth profile showed narrower pores for the top silica layer.
- PALS showed broader pores for the silica layer closer to the interlayer.
- Increasing the surfactant loading reduced He/CO_2 selectivity from 91.5 to 3.8.
- PALS pore size profile corelated well to selectivity based on surfactant loading.

Surfactant functionalized cobalt silica membranes – gas permeation and thin film positron annihilation lifetime spectroscopy characterisation

Gianni Olguin[1,2*], Christelle Yacou[1,3], J. Motuzas[1], Maik Butterling[4], Wilhelm A. Meulenberg[5], Simon Smart[1], João C. Diniz da Costa[1,6,7*]

Graphical Abstract

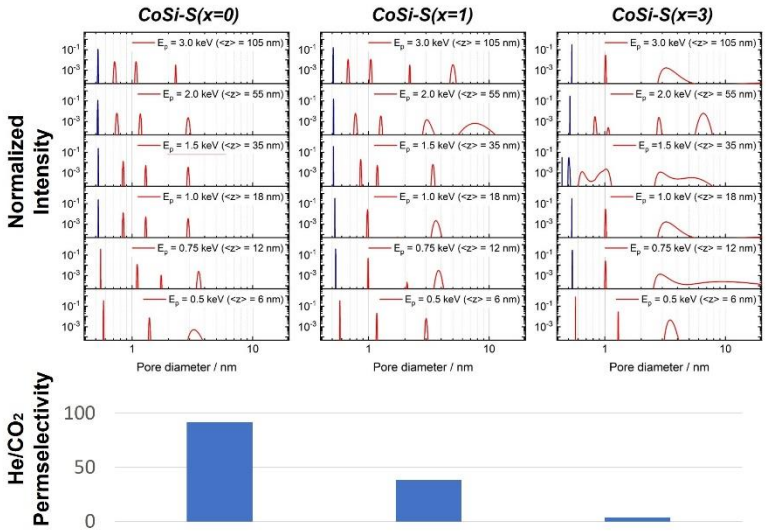

Surfactant functionalized cobalt silica membranes – gas permeation and thin film positron annihilation lifetime spectroscopy characterisation

Gianni Olguin[1,2*], Christelle Yacou[1,3], J. Motuzas[1], Maik Butterling[4], Wilhelm A. Meulenberg[5], Simon Smart[1], João C. Diniz da Costa[1,6,7*]

[1]The University of Queensland, FIM[2]Lab – Functional Interfacial Membranes and Materials Laboratory, School of Chemical Engineering, Brisbane Qld 4072, Australia.

[2]Pontificia Universidad Católica de Valparaíso, Escuela de Ingeniería Química, Valparaíso, Chile.

[3] Laboratory COVACHIM-M2E, EA 3592, Université des Antilles, BP 250, 97157 Pointe-à-Pitre, Guadeloupe, France.

[4]Helmholtz-Zentrum Dresden - Rossendorf, Institute of Radiation Physics, Bautzner Landstraße 400, 01328 Dresden, Germany

[5]Forschungszentrum Jülich, Institute of Energy and Climate Research (IEK - 1), Wilhelm - Johnen - Strasse, 52425 Jülich, Germany

[6]LAQV-REQUIMTE, (Bio)Chemical Process Engineering, Department of Chemistry, Faculty of Science and Technology, Universidade NOVA de Lisboa, 2829-516 Caparica, Portugal.

[7]iBET – Instituto de Biologia Experimental e Tecnológica, 2781-901 Oeiras, Portugal.

Abstract

This work investigates the use of positron annihilation lifetime spectroscopy (PALS) for the in-situ structural characterisation of silica derived thin film membranes. By using a quantified maximum entropy method, PALS allowed for the measurement of porous volumetric fraction and a pore size distribution depth profile. PALS measurements were carried out on a series of silica derived membranes where alumina supports were coated with four layers of cationic HTBA surfactant cobalt silica sols wherein the surfactant / cobalt molar ratio loading varied from 0 to 3. PALS results showed

that the coated layers adjacent to the porous alumina substrate were characterised by micropores and broad mesopores, a clear indication that the porosity of the substrate affected the pore size at the substrate and thin film interface. The last coated layer resulted in narrow micropores with a trimodal pore size distribution of 0.5-0.6 nm, ~1nm and ~3nm. This was attributed to the surface smoothness conferred by three previous coated layers. The increase in the surfactant loading led to an increase in the pore fraction of thin films as ascertained by PALS. These results correlated quite well with the gas permeation and selectivity results. Higher surfactant loadings resulted in an increase is gas permeation and reduction of He/CO_2 selectivity from 91.5 to 3.8. PALS proved to be a powerful tool characterisation of the structural features of microporous thin films.

Keywords: silica membranes; surfactant; pore size; thin film; gas permeation.

1. Introduction

Gas separation is a major chemical engineering process, important to a wide variety of industries, where removal of undesirable species or concentration of products is desirable. There are many processes used for gas separation such as (i) cryogenics involving very low temperatures and changing phase from gas to liquid [1, 2]; (ii) adsorption processes requiring gas cooling to room temperatures to take advantage of sorbents sorption capacities at low temperatures [3, 4]; (iii) absorption processes where gases react with solvents thus requiring a downstream desorbing processing [5, 6]; and (iv) membranes which can separate gases without phase change [7]. As many industrial gases are generated at high temperatures and high pressures the use of inorganic membranes, which are chemically and thermally stable, is attractive [8]; particularly palladium alloys [9] and molecular sieving silica [10-12]. Of particular attention cobalt oxide silica membranes have been scaled up with proven performance for 2000 hours operation and reaching very high H_2/CO_2 permselectivities of 500 [13].

Metal oxide silica membranes are synthesised from a silica sol-gel method using hydrated metal nitrates which are oxidised during synthesis. Embedding cobalt oxide into silica films conferred functionalities otherwise not available in pure silica membranes, such as improvements for wet gas separation [14-16], although the mechanism of protection was not clear. More recently, work by Liu and co-workers [17, 18] reported that the Co^{3+} coordination with Si increased hydro-stability, whilst hydrolytic attack was severe on membranes containing a higher concentration of Co^{2+} coordinated with Si. The literature contains a multitude of metal oxides incorporated into silica thin films from the initial examples of oxides of nickel [19, 20], to aluminium [21], zirconium [22], titanium [23], niobium [24], and more recently binary oxides of cobalt with iron [25], palladium [26] and lanthanum [27].

Different oxides also confer different functionalities to the resultant membranes. For instance, niobium oxide silica membranes provided relatively good N_2/CO_2 permselectivity of ~8 [28], higher than any previous silica membranes of values below 2-3. In the case of adding lanthanum to a CoSi membrane, it allowed the formation of silicates which enhanced the thermal stability of the pore sizes below 3Å under reduction and oxidation cycles [26]. In another case, Ji et al. [29] demonstrated that pore connectivity of CoSi membranes increased as the membranes were reduced using a H_2 rich atmosphere at high temperatures. This was attributed to the effect of the gas to solid reaction of H_2 to the cobalt oxide particle (Co_3O_4) which was reduced to CoO. During reduction, cobalt oxide particles breaks into small particles, known as the crackling core model [30, 31], and formed additional permeation channels.

In the pursuit of additional functionalities, Olguin and co-workers [32] reported that the oxidation state of cobalt oxide could be tailored by the halide functionality of surfactants in silica gels. Whilst this work focused on xerogels, surfactants and carbon templates have been previously used for the preparation of silica membranes. For instance, Verweij and co-workers [33] carbonised a ligand

methyl group to silica precursors which improved the hydro-stability of the silica membranes. Duke et al. [34] carbonised surfactants embedded in silica xerogels and showed that the carbon moieties were like barriers opposing the movement of unstrained silica groups, thus avoiding densification under hydrothermal conditions. In a further work, Olguin et al. [35] showed that the length of the alkyl group and the surfactant concentration influenced the porous structural formation of cobalt oxide silica xerogels.

The published works on the effect of surfactants on CoSi has been limited to xerogel studies, whilst membranes have yet to be fully reported. This is an important point as the chemical and physical principles that control the silica structural formation are, in theory, the same for both bulk xerogels and thin films. However, the latter undergoes fast gelation and evaporation of solvents (i.e. water), and the final structure of surfactant functionalised CoSi thin films may differ from that of bulk xerogel. A characterisation technique to study thin films in membranes is positron annihilation spectroscopy (PALS) that has been reported for polymeric membranes [36-38], and crystalline inorganic (i.e., zeolite) membrane [39]. In the case of amorphous silica membranes, publications on in situ characterisation of silica thin films supported by substrates is even more limited as in principle the silica sol-gel solution slightly penetrates into the pores of interlayer due to capillary forces during film coating.

Therefore, this work investigates two important aspects of silica derived membranes. The first investigation focuses on determining the pore structure of supported thin films using PALS. The second investigation studies the performance of surfactant functionalised CoSi membranes for gas separation. Hexyl trimethyl ammonium bromide (HTAB) was chosen as the functional surfactant in view of its effect in the oxidation state of CoSi xerogels [35]. A series of membranes were prepared via a sol-gel synthesis method, where the concentration of HTAB was varied. Single gas permeation of He, H_2, N_2 and CO_2 was performed for each of the prepared membranes at different testing

temperatures in the range 200-500 °C. This work is particularly interested in understanding how the surfactant functionalities on CoSi membranes in terms of porosity and pore sizes as determined by PALS can affect gas transport phenomena and membrane performance.

2. Experimental

Cobalt silica (CoSi) coating solutions were synthesised via a sol-gel method. Cobalt nitrate hexahydrate ($Co(NO_3)_2.6H_2O$) was dissolved in 30 %vol hydrogen peroxide (H_2O_2) in order to keep the pH stable around 3.0 and then diluted in an excess of ethanol. Subsequently, the solution was cooled to 0 °C, followed by a slow drop-wise addition of tetraethyl orthosilicate (TEOS). The final TEOS : H_2O : H_2O_2 : EtOH : $Co(NO_3)_2.6H_2O$ molar ratios was 4 : 45.5 : 9 : 256 : 1, which was moderately stirred in an ice-bath at 0 °C for three hours. The preparation of surfactant cobalt silica followed the same procedure, except for the addition of hexyl trimethyl ammonium bromide (HTAB) after the ice-bath treatment. Surfactant concentration was varied based on the surfactant/cobalt molar ratio (*x*) 0 to 3 and the resultant sols were named as CoSi-S(x). The HTAB concentration variation aimed at varying the pore size and pore volume of the resultant CoSi membranes based on homologue xerogels published elsewhere [32, 35]. The solubility of surfactant was achieved by keeping the concentration below the critical micelle concentration (CMC) point, taking into account the surfactant type [40], solvent nature [41, 42] and counter ion presence [43]. The HTAB concentration in our surfactant-cobalt silica sol was varied from 0 (*x=0*) to 180 mM (*x=3*) below the CMC of 2000 mM.

Membranes were prepared by dip coating four active silica layers on outer shell of a commercial alumina substrate (Energy Research Centre of the Netherlands). The dimensions of the tubes were 14 mm external diameter with 2 mm thick wall, a length of 200 mm. The tubes contained an asymmetric structure, with α-alumina substrate followed by small α-alumina particle interlayers, and thin γ-alumina interlayers with 4nm pore sizes. A conventional dip coater was used to coat silica layers through a constant immersion and withdrawal speed of 10 cm min^{-1} and dwell time of 1 min. Each

silica layer was subsequently calcined in an electric furnace at 630 °C under air atmosphere, a ramping rate of 1 °C min^{-1} and a dwell time of 2.5 hr. Under these calcination temperatures, the HTBA is fully burnt off [32], resulting in the formation of a surfactant free CoSi membranes.

The performance of each membrane was assessed by single gas permeance of He, H_2, N_2 and CO_2 at four different operation temperatures (200, 300, 400 and 500 °C) in a custom permeation rig (see Fig. 1). The permeate stream was kept at atmospheric pressure while feed pressure was set constant at 400 kPa. A series of leaking tests were run each time before membrane testing, to ensure that any problems associated with seal failure or membrane fractures were not present. The leaking tests involved checking gas leaks in valves and connections in the gas permeation rig and membrane module. The membrane was sealed using graphite seals developed by Yacou and co-workers [13], that allows gas permeation testing at high temperatures without sheering ceramic tubes. The membranes with high gas permselectivities were considered gas leak free and defect free.

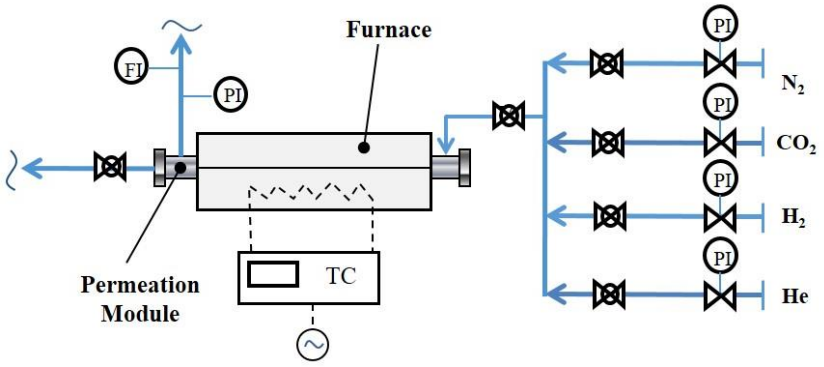

Fig. 1 - Single gas permeation rig: pressure regulator (PI), flow rotameter (FI), temperature controller (TC).

Positron annihilation lifetime spectroscopy (PALS) experimental set up required a flat and homogeneous surface for thin film analysis since the probing positron beam has a diameter of around 5 mm. Therefore, PALS was carried on flat alumina supports made of α-alumina substrate and a thin layer of γ-alumina (supplied by Pervatech) with 80 nm pore size. Each support was dip coated with

4 active silica layers on a custom coater, taking into consideration similar parameters to the tubular membranes. The calcination procedure for each layer was the same as for the tube membranes. Samples of the latter were analysed by a field emission scanning electron microscope (JEOL Model JSM-7001F) to observe their morphological features. The analysis was performed using a 5kV acceleration voltage and a distance of 10 mm.

The PALS experiments were performed at the mono-energetic positron source (MePS) beamline, which is one of the end stations of the radiation source ELBE (Electron Linac for beams with high Brilliance and low Emittance) at HZDR (Germany) [44, 45], using positrons produced from high-energy bremsstrahlung of the 30 MeV electron source ELBE. The PALS spectra were recorded using a fast $CeBr_3$ scintillator detector coupled to a Hamamatsu R13089-100 PMT. After implantation into a solid, positrons lose their kinetic energy due to thermalization and, after a short period of diffusion, annihilate in delocalized lattice sites or localize in vacancy-like defects and pores, emitting usually two anti-collinear 511 keV gamma photons after annihilation with the encountered electrons. The implantation profile can be calculated via a Makhovian distribution [46] (see Appendix Fig. A1). A mean positron implantation depth can be approximated by a simple material density-dependent, Makhovian positron stopping profile formula [42]: $\langle z \rangle = 36/\rho \cdot E_p^{1.62}$, with the material density, ρ and positron implantation energy, E_p. Positron implantation energy was varied from 0.5 to 12 keV providing an approximated depth profile between 0 and 100 nm.

Positron lifetime components were obtained through a quantified maximum entropy method. The porous volumetric fraction of surfactant functionalised silica layers was calculated averaging the shortest lifetime component (related with annihilation within material) along with silica thickness. The pore size distribution (PSD) depth profile is based on the positron energy which changes with the implantation depth (see Appendix Fig. A1), and allows the pore size of the sub-layers to be analysed and determined. The collected data are known as PALS lifetime distribution, given by the

annihilation versus lifetime value for each implantation depth. The PALS lifetime distribution represents multiple cavities sizes in the surfactant functionalised silica membrane, thus requiring deconvolution to determine the pore size of the cavities (see Appendix Fig. A2). Deconvolution is carried out using non-standard gaussian peaks to get lifetime components (τ_5, τ_4, τ_3…) which can be translated into pore sizes according to a simple shape-free model based on the extended Tao-Eldrup model for pore size determination from PALS [47] (see Appendix Fig. A3). For each spectrum $3x10^6$ counts were recorded at a rate of 3600 counts per second, for positron implantation energies from 0.5 keV to 12 keV (Appendix Fig. A4). Positron lifetime components were then obtained based on the maximum entropy method using the MELT (maximum entropy lifetime analysis) software package [48]. In contrast to a discrete lifetime analysis using multi-exponential decay functions, a MELT analysis allows to extract pore size distributions rather than only discrete pore sizes as detailed in the Appendix.

3. Results

3.1 Characterisation

Representative SEM images of the as-prepared membrane are depicted in Fig. 2. The cross-section is composed of a surfactant functionalised cobalt silica top layer coated on a γ-Al_2O_3 interlayer. The latter was coated on a macroporous α-Al_2O_3 substrate characterised by a coarse surface containing large particles. The interlayer is required to reduce the roughness of the substrate surface to enable coating of the top layer. The top layer has a homogeneous surface coverage in all directions with a thickness of ~120 nm. A total of four surfactant cobalt layers were coated on the substrate, suggesting that each coated layer resulted in a thickness of ~30 nm upon calcination.

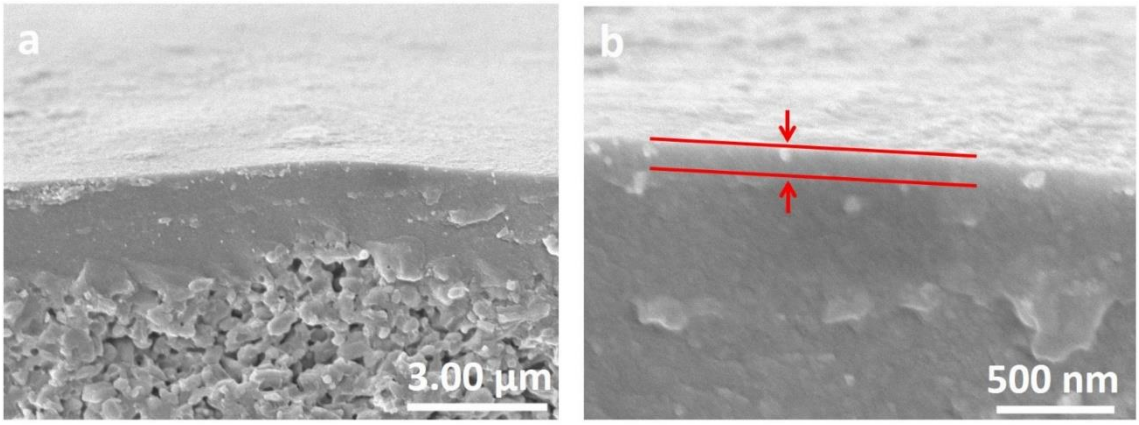

Fig. 2. Representative SEM image of surfactant functionalised cobalt silica membrane.

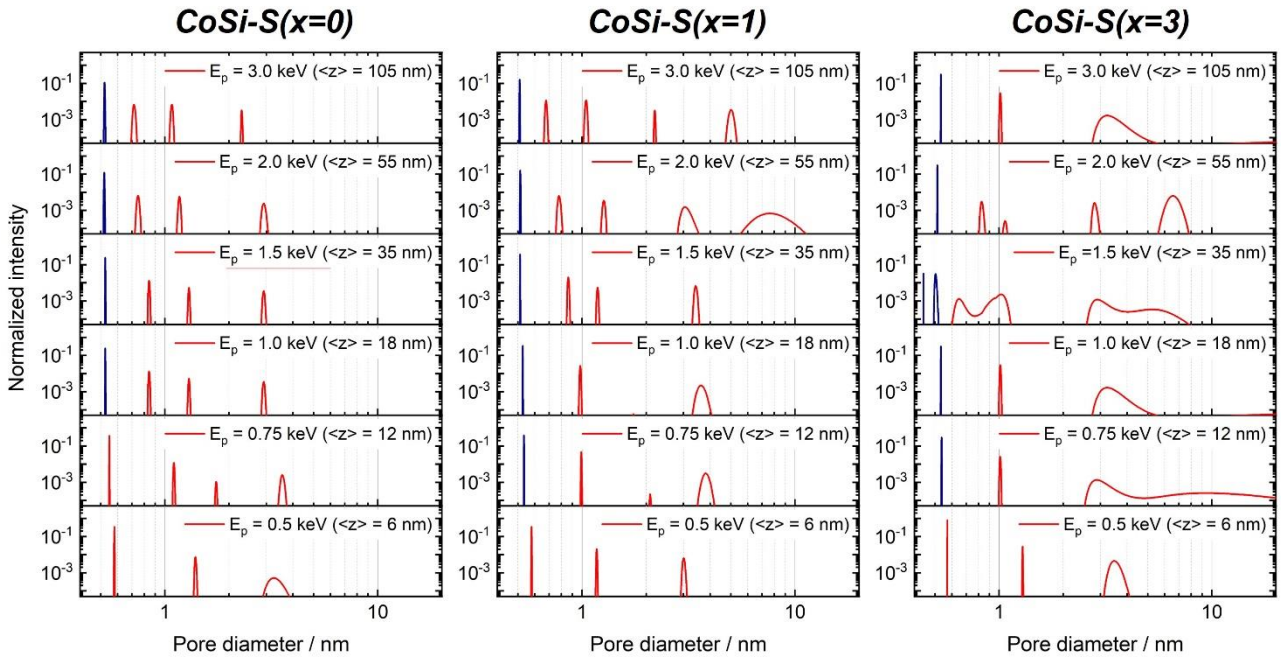

Fig. 3. Positron pore size distribution for different positron implantation energies E_p for a surfactant functionalised CoSi membranes. The mean implantation depths <z> are calculated from the Makhovian stopping profiles using $\langle z \rangle = 36/\rho \cdot E_p^{1.62}$. Usually, positrons are implanted in a much wider depth range (see appendix Fig. A1), therefore the given values are just a rough estimation. The blue narrow peak around 0.5 nm is not a signal from annihilation in pores but from free positrons annihilating in the matrix material. Although this lifetime component is not related to a pore, the peak is shown here in the figure for comparing free positron annihilation and annihilation in pores.

196

197 Fig. 3 displays PSD profiles along the depth of the surfactant functionalised cobalt silica membranes.
198 The PSD profile shows a relative abundance of pore sizes at each depth, grouped as micropores ($d_p <$
199 2 nm) and mesopores ($2 \leq d_p \leq 50$ nm). The presence of a tri-modal PSD at depths up to 18 nm, are
200 in line with the PALS work pioneered by Duke et al. [49] for silica powders. Importantly though, the
201 top portion of fourth and final coated layer (from 0 to ~ 30 nm) for membranes *x=0* and *x=1* showed
202 high intensity peaks at $d_p < 2$ nm as compared to larger implantation depths, reflecting a shift to
203 micropore PSD. This is attributed to the surface smoothness of the previous coated and calcined
204 surfactant functionalised silica layers. It strongly indicates that four layers were sufficient to produce
205 a defect free thin film. The membrane *x=3* exhibited a higher contribution of peaks at $d_p > 2$ nm, a
206 clear indication of the formation of mesopores. This is attributed to higher concentration of HTAB
207 that are burnt off upon calcination, contributing to pore size enlargement.
208

209 Beyond a film depth of >35nm (for the 2nd and 3rd coated layers to be precise) the intensity of the
210 peaks associated with mesopores broadens for membranes *x=0* and *x=1*, confirming the incorporation
211 of more mesopores into the CoSi thin film layers. The increase in the contribution of mesopores may
212 be associated with morphological effects which stem from the underlying larger pores in the substrate.
213 However, the drying and calcination process is clearly complex as the first coated layer at a PALS
214 depth of 105 nm actually showed a lower mesopore contribution than the 2nd and 3rd layers (at 55nm
215 and 35nm respectively). Similarly, the membrane *x=3* also displayed a reduction of the contribution
216 of mesopores. In this case, the PSD may be associated with the intrusion of the surfactant cobalt silica
217 sol into the mesopores of the interlayer.
218

219 The determination of the PSD depth profile also allowed for the calculation of the positron porosity
220 fraction as displayed in Fig. 4. The porosity fraction is the fraction of all positrons annihilating in

221 micro- and mesopores. Remaining positrons are annihilating as free positrons (see blue peak in Fig.
222 3). Fig. 4 displays the pore values as PALS porosity fraction and pore volumes determined from
223 nitrogen sorption isotherms. It is observed that by increasing the surfactant ratio (*x*) used to prepare
224 the functionalised surfactant cobalt silica thin films, the positron porosity fraction likewise increased.
225 The surfactant molecules act as templates or free-volume spaces embedded into the cobalt silica
226 matrix. Upon calcination in air, the surfactant is fully burnt-out at 530 and 550 C [32] for membranes
227 *x=1*and *x=3*, respectively. By raising the calcination temperature further, the porous cobalt silica thin
228 film densifies, and the positron porosity fraction was linear with respect to the surfactant ratio.

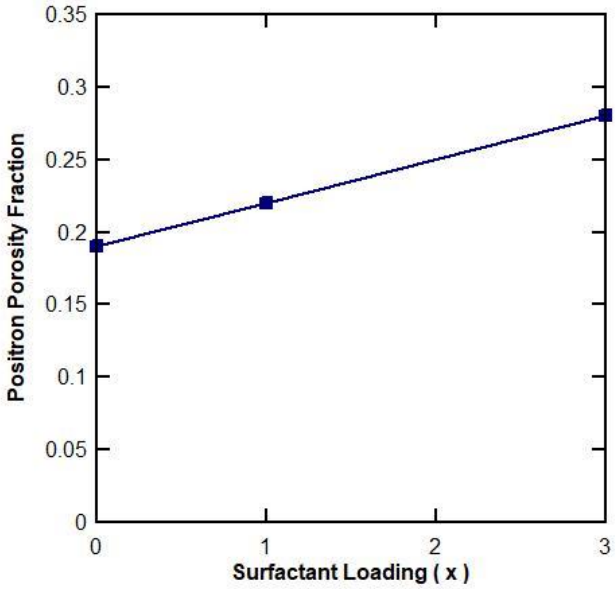

229

230 Fig. 4. Positron porosity fraction as a function of the surfactant ratio (*x*) used to prepare the
231 functionalised surfactant cobalt silica membranes.

232 **3.2 Gas permeation**

233 Fig. 5 shows the single gas permeance of He, H_2, N_2 and CO_2 gases at various temperatures for three
234 tested membranes. The CoSi (*x*=0) membrane, with no surfactant loading, follows the traditional
235 temperature dependent gas transport as reported elsewhere for cobalt silica membranes [13, 50] and
236 silica membranes [51, 52] based on the transport of gases in microporous materials [53]. This
237 membrane is characterised by the permeance of the smaller gases, He (d_k=2.6 Å) and H_2 (d_k=2.89 Å),

increasing with temperature, whilst the permeance of the larger gases, CO_2 (d_k=3.3 Å) and N_2 (d_k=3.64 Å), decreased with temperature. Similar behaviour was observed for the SCoSi (x=1), though the larger gases showed almost no decline in permeance as the testing temperature was raised. By adding more surfactant as SCoSi (x=3) membrane, the single gas transport behaviour changed. For instance, gas permeance in this x=3 membrane remains steady as a function of the temperature, within experimental error of ±8%. Further, the single gas permeation curves for the smaller and larger gases are much closer, and not as distanced as for the lower surfactant loaded membranes (x=0 and 1). The results in Fig. 5 strongly suggest that surfactant loading is conferring morphological changes to the final structure of the cobalt oxide silica membranes.

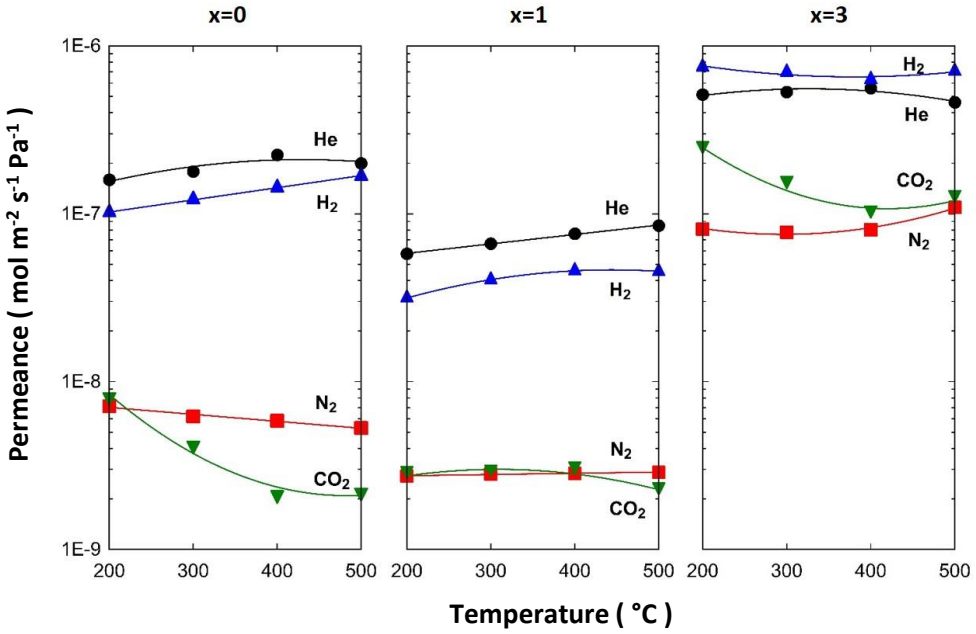

Fig. 5. Single gas permeance (±8%) as a function of temperature for membranes with varied surfactant loading (x).

The temperature dependent transport observed in Fig. 5 is also known as activated transport based on Barrer's model [54] for gas diffusion via microporous structures. Fig. 6 shows the apparent energy of activation (E_{act}) for H_2 and N_2 as a function of surfactant loading. The E_{act} was calculated from the Arrhenius plot of the permeance of for H_2 and N_2. In principle, E_{act} gives a good indication of pore

size changes provided that gas permeation follows activated transport. For instance, smaller micropores are characterised by higher He and lower N_2 E_{act} values. This is clearly observed for membranes *x=0 and 1*. However, membranes *x= 3* shows that a convergence of both E_{act} values, given a clear indication of increased pore sizes. This shows a departure from activated transport to Knudsen diffusion, a characteristic of pore size change from micropore to mesopore. These results correlated well with the positron PSD in Fig. 3.

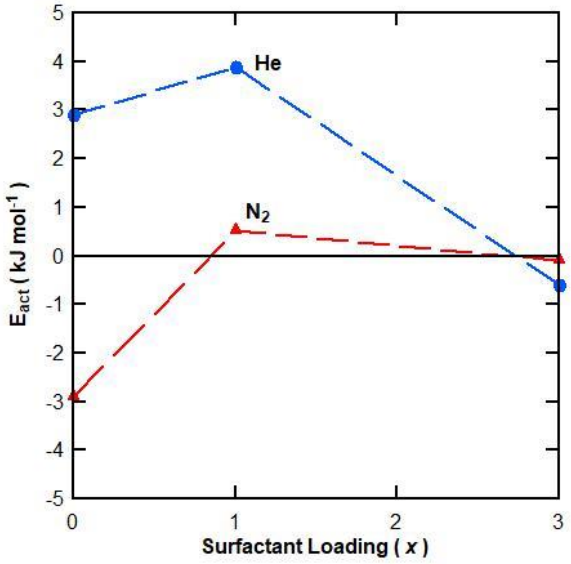

Fig. 6. Apparent energy of activation (E_{act}) for H_2 and N_2

Fig. 7a displays the permselectivity of several gas pairs at 500 ^oC. The permselectivity was determined from the ratio of the permeance of each gas pair. It is interesting to observe that membrane *x=0* showed higher He/CO_2 (91.5) and H_2/CO_2 (77.0) as compared to He/N_2 (37.7) and H_2/N_2 (31.8). Considering that the kinetic diameter of CO_2 (d_k=*3.3 Å*) is smaller than that N_2 (d_k=*3.64 Å*), the permselectivity should be higher for gas pairs containing N_2 instead of CO_2 for molecular sieve membranes. Nevertheless, this is attributed to the adsorption effect in ultramicroporous silica membranes such as membrane *x=0*. The isostheric heat of adsorption Q_{st} in CoSi membranes for CO_2 (Q_{st} = *22.7 kJ mol^{-1}*) [29] is higher than N_2 (Q_{st} = *5 kJ mol^{-1}*) [50]. Q_{st} represents an energy barrier

and higher values leads to the reduction of permeance as a function of temperature as observed in Fig. 5 for membrane x=0. As the pore sizes increase, adsorption becomes less prevalent and permselectivity decreases as observed for membrane x=1. In the case of membrane *x=3*, the permselectivity for the gas pairs converged to similar values, confirming the enlargement of pore sizes as observed in the positron PSD (Fig. 3).

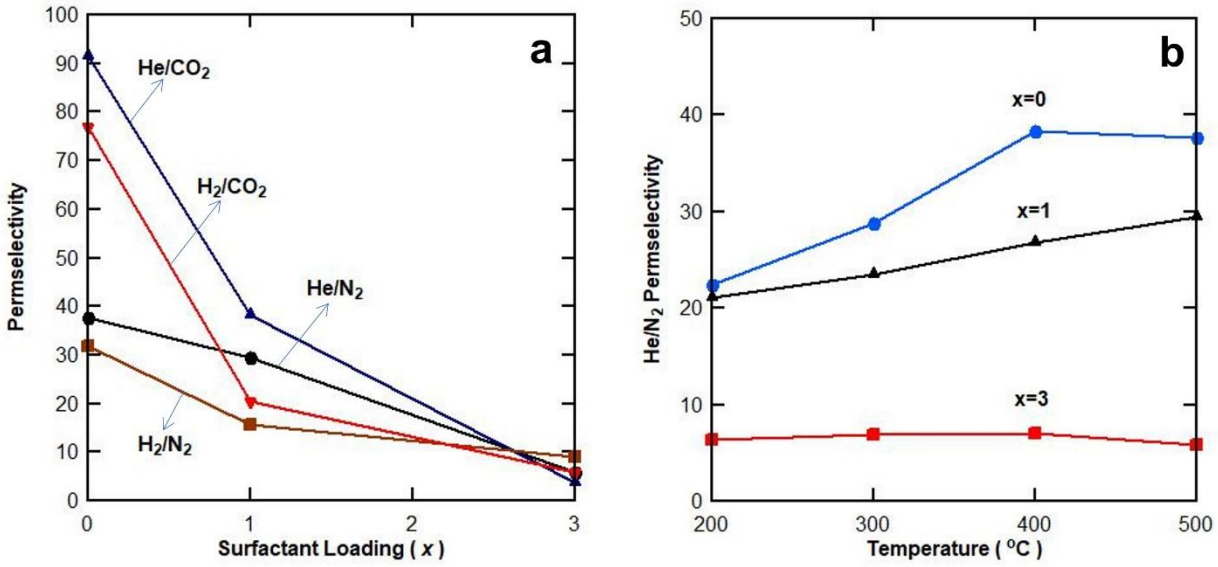

Fig. 7. (a) Permselectivity of gas pairs at 500 °C as a function of membrane surfactant loading, and (b) He/N_2 permselectivity for all membranes as a function of temperature.

Fig. 7b shows the He/N_2 permselectivity for all membranes as a function of temperature. Helium is a non-adsorbable gas [55] under the testing conditions in this work. The increase in He/N_2 as a function of temperature reflects the effect of N_2 adsorption for membranes *x=0 and 1*. The He/N_2 permselectivity is low for *x=3*, around 6.5 and remained almost constant. As the ideal Knudsen selectivity of He/N_2 is 2.6, the low permselectivity strongly suggest that the transport phenomena behaviour changed from molecular sieving for SCoSi (*x=0 and 1*), to Knudsen transport for SCoSi (*x=3*). This is in line with the pore size broadening, where silica apertures control the passage of

gases. This result correlates well with the positron PSD (Fig. 3) for membrane *x=3*, evidenced by the contribution of mesopores in the CoSi thin films.

To understand further the morphological features of the membranes in this work, the average pore sizes calculated from PALS SCoSi thin film measurements (Fig. 3) are compared against those obtained for homologue xerogels from conventional N_2 sorption. Fig. 8 shows the He/N_2 at 500 °C plotted as function of pore sizes for PALS and N_2 sorption. It is well known that the pore size in microporous membranes control the separation of gases of different kinetic diameters. This is true for both measurements as He/N_2 permselectvities decrease as pore sizes increase. However, it is observed in Fig. 8 that pore sizes obtained from N_2 sorption display small variations from 2.1 to 2.4 nm as the surfactant load was raised from x=0 to 3, respectively. PALS measurements showed a better resolution as pore sizes varied from 1.2 to 3 nm in the same range of surfactant loading.

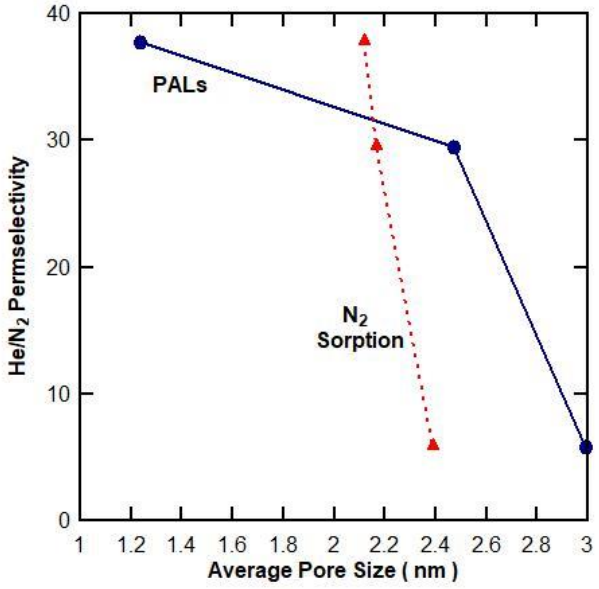

Fig. 8. He/N_2 permeance at 500 °C as a function of average pores based on PALs (blue circles-solid line) for membranes calcined at 630 °C and N_2 sorption for xerogels calcined at 600 °C [32] (red triangles-dashed line). Lines are provided to better identify the two data series.

Morphological differences stemming from PALS and N_2 sorption measurements are observed further in Fig. 9. In principle, if pore fraction or pore volume increases, then the trend is for permeation to increase too as there is less resistance for gas transport through the membrane. Indeed, this is the case for the PALS measurements though the initial point is slightly scattered but within the permeation experimental error of 8%. In the case of pore volumes from N_2 sorption, the permeation results buck this trend in this work. Both He and N_2 permeance have similar pore volumes for the surfactant sols x=1 and 3, but the differences in permeance results are 5.5 and 33 times, respectively.

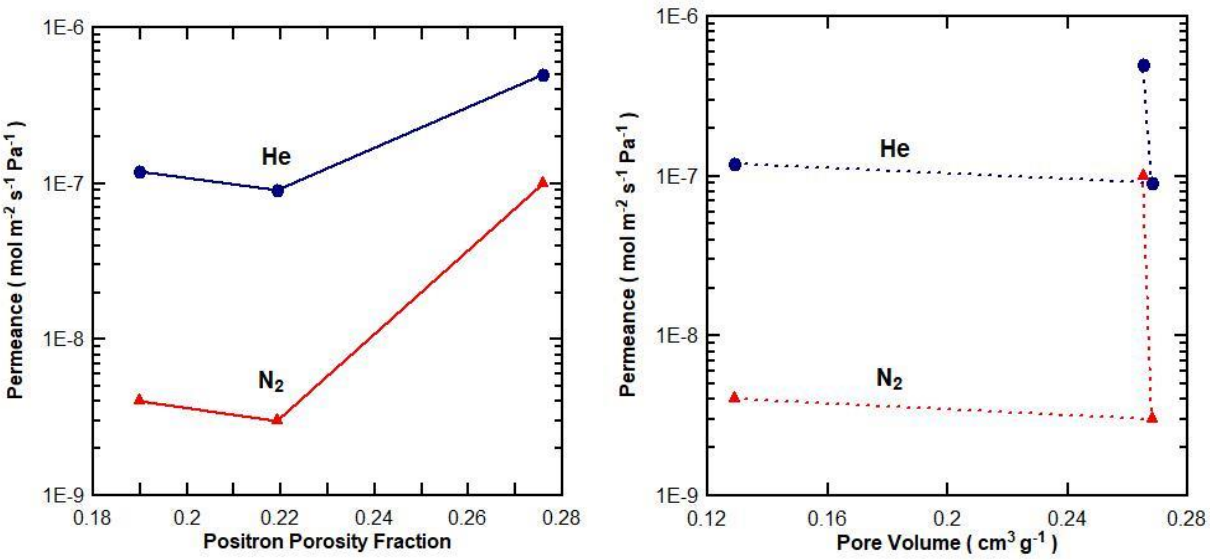

Fig. 9. He and N_2 permeance at 500 °C as a function of (a) positron porosity faction determined from PALS for membranes calcined at 630 °C and (b) pore volumes determined from N_2 sorption isotherms for xerogels calcined at 600 °C [32]. Lines are provided to better identify the two data series.

Figs. 8 and 9 clearly show that PALS measurements provide better precision for thin films based on permeation properties. Although the underlying physics and chemistry that govern silica growth and gelation are essentially the same for films as bulk gels, other factors influence structural evolution in films [56]. For instance, the properties of a deposited thin film may be quite different due to non-equivalent gelation and drying conditions [57, 58]. The PALS results in this work clearly show that the morphological features of silica derived thin films and xerogels are different, thus addressing

these important and valid points raised by Brinker and co-workers [56, 57] and Meixner and Dyer [58] over two decades ago.

4 Conclusions

PALS characterisation of surfactant loaded CoSi thin films showed a higher contribution of micropore formation on the top layer, to a depth of ~12 nm. The PSD tended to show an increased fraction of micropores and mesopores at higher penetration depths (i.e., closer to the porous alumina interlayer), suggesting the substrate porosity affected the pore formation in the adjacent membrane layers. Gas permeation testing confirmed that the incorporation of a cationic surfactant as a secondary dopant component on cobalt containing silica altered separation performance. High loads of surfactant increased gas permeance resulting in reduced selectivities, a demonstration of pore size increase. The permeation and selectivity results are consistent with the PALS measurements where the porosity fraction and pore sizes also increased with the surfactant load of the prepared membranes. PALS measurement of thin films structural features is powerful characterisation tool that showed strong correlations the transport properties of the surfactant CoSi membranes.

Acknowledgment

The authors would like to acknowledge funding support from the Australian Research Council through Discovery Project Grant DP110101185. G. Olguin acknowledges funding support from the bicentenary scholarship program from the Chilean Government and Jan S. Eiberger from the Forschungszentrum Jülich in Germany regarding discussions on PALS. J. C. Diniz da Costa gratefully thank the support given by the Australian Research Council Future Fellowship (FT130100405) program and the grant as invited Professor funded by the Associate Laboratory for Green Chemistry – LAQV, financed by the National Portuguese funds from FCT/MCTES (UIDB/50006/2020).

Competing interests

The authors declare no competing interests.

Appendix

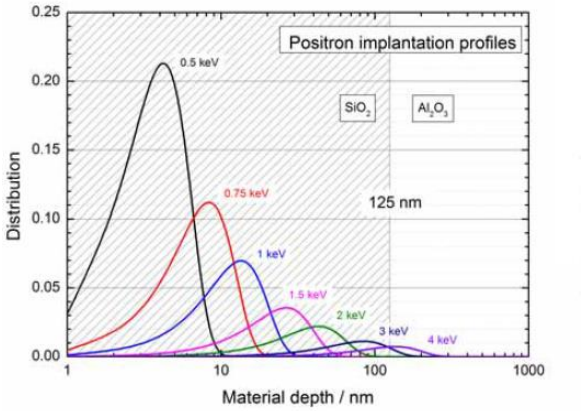

Fig. A1. Implantation depth profile versus positron energy for the case of SiO_2 on Al_2O_3 [42].

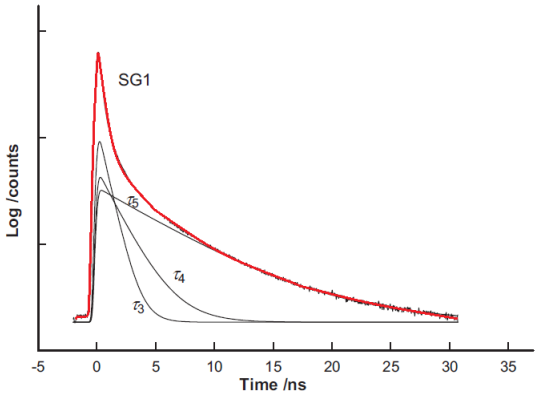

Fig. A2. Deconvolution of the positron annihilation lifetime spectrum of a surfactant functionalised cobalt silica membrane (*x=1*) [49].

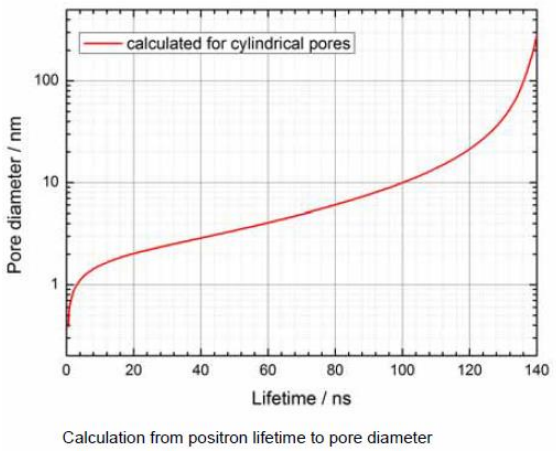

Fig. A3. Plot for calculation of pore diameter based on positron lifetime according to a shape-free model, based on the extended Tao Eldrup model [43].

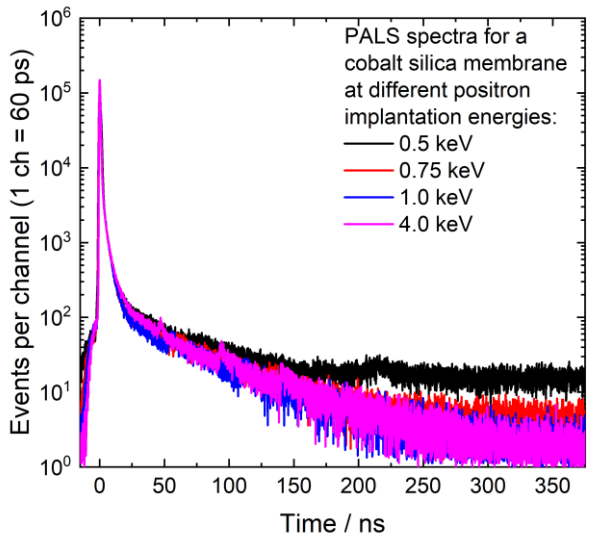

Fig. A4. Exemplary Positron Annihilation Lifetime spectra of a surfactant functionalised cobalt silica membrane (*x=1*) for different positron implantation energies.

Within the maximum entropy method, the entropy weight parameter *a* controls the competition between entropy solution and data constraints [48]. For a = 0, the solution is the pure least squares fitting result obtained by the standard PALS analysis using a multi-exponential decay approach. By

varying *a*, a series of solutions with different probabilities is obtained where usually the solution with the largest probability is chosen (Fig. A5).

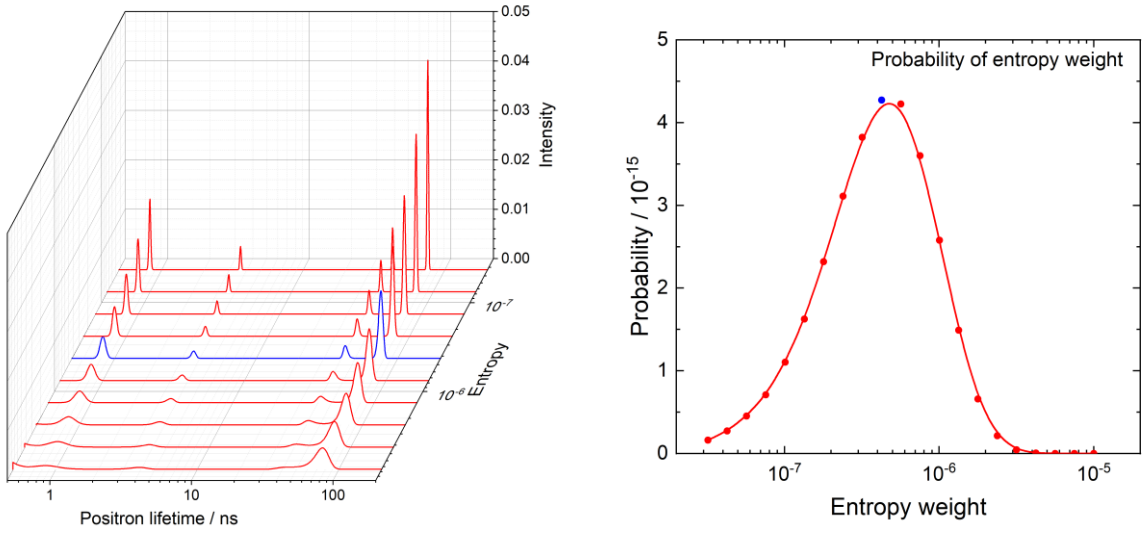

Fig. A5. Exemplary MELT analysis of a surfactant functionalised cobalt silica membrane recorded at positron energy of 6 keV (mean implantation depth 320 nm) with solutions for different entropies (left) and the probability for each entropy weight (right). The blue curve (left) and dot (right) are the chosen solutions with the maximum entropy.

References

[1] A.R. Smith, J. Klosek, A review of air separation technologies and their integration with energy conversion processes, Fuel Proc. Technol. 70 (2001) 115-134.

[2] M.A. Moreira, A.M. Ribeiro, A.F.P. Ferreira, A.E. Rodrigues, Cryogenic pressure temperature swing adsorption process for natural gas upgrade, Sep. Purif. Technol. 173 (2017) 339-356.

[3] S.K. Wirawan, D. Creaser, Multicomponent H_2/CO/CO_2 adsorption on BaZSM-5 zeolite, Sep. Purif. Technol. 52 (2006) 224-231.

[4] N.N. Linneen, R. Pfeffer, Y.S. Lin, CO_2 adsorption performance for amine grafted particulate silica aerogels, Chem. Eng. J. 254 (2014) 190-197.

[5] F.J. Tamajón, Estrella Álvarez, Fernando Cerdeira, Diego Gómez-Díaz, CO_2 absorption into N-methyldiethanolamine aqueous-organic solvents, Chem. Eng. J. 283 (2016) 1069-1080.

[6] Q. Ye, L. Zhu, X. Wang, Y. Lu, On the mechanisms of CO_2 absorption and desorption with phase transitional solvents, Int. J. Greenhouse Gas Cont. 56 (2017) 278-288.

[7] D. S. Sholl, R. P. Lively, Seven chemical reactions to change the world, Nature 532 (2006) 435–437.

[8] S. Smart, C.X.C. Lin, L. Ding, K. Thambimuthu, J.C. Diniz da Costa, Ceramic membranes for gas processing in coal gasification, Energy Environ. Sci. 3 (2010) 268–278.

[9] N.A. Al-Mufachi, N.V. Rees, R. Steinberger-Wilkens, Hydrogen selective membranes: A review of palladium-based dense metal membranes, Renewable Sustain. Energy Rev. 47 (2015) 540-551.

[10] N.W. Ockwig, T.M. Nenoff, Membranes for hydrogen separation, Chemical Rev. 107, 2007, 4078-4110.

[11] P. Bernardo, E. Drioli, G. Golemme, Membrane Gas Separation: A Review/State of the Art, Ind. Eng. Chem. Res. 48, 2009, 4638-4663.

[12] N. Moriyama, H. Nagasawa, M. Kanezashi, T. Tsuru, Selective water vapor permeation from steam/non-condensable gas mixtures via organosilica membranes at moderate-to-high temperatures, J. Membr. Sci. 589 (2019) 117254.

[13] C. Yacou, S. Smart, J. C. Diniz da Costa, Long term performance of a multi-tube cobalt oxide silica membrane at high temperatures for gas separation, Energy Environ. Sci. 5 (2012) 5820–5832.

[14] R. Igi, T. Yoshioka, Y.H. Ikuhara, Y. Iwamoto, T. Tsuru, Characterization of co-doped silica for improved hydrothermal stability and application to hydrogen separation membranes at high temperatures, J. Am. Ceram. Soc., 91 (2008) 2975-2981.

401 [15] S. Battersby, B. Ladewig, S. Liu, M.C. Duke, V. Rudolph, J.C. Diniz da Costa, Hydrothermal
402 stability of cobalt doped silica membranes in a water gas shift membrane reactor, Sep. Purif.
403 Technol. 66 (2009) 299–305.
404 [16] D. Uhlmann, S. Smart, J. C. Diniz da Costa, High Temperature Steam Investigation of Cobalt
405 Oxide Silica Membranes for Gas Separation, Sep. Purif. Technol. 76 (2010) 171–178.
406 [17] L. Liu, D.K. Wang, D.L. Martens, S. Smart, J.C. Diniz da Costa, Influence of the cobalt phase
407 sol-gel conditioning on the hydrothermal stability of cobalt doped silica membranes, J. Membr.
408 Sci. 475 (2015) 425–432.
409 [18] L. Liu, D.K. Wang, P. Kappen, D.L. Martens, S. Smart, J.C. Diniz da Costa, Hydrothermal
410 stability investigation of microporous silica containing long-range ordered cobalt oxide clusters
411 by XAS, Phys. Chem. Chem. Phys. 17 (2015) 19500-19506.
412 [19] M. Kanezashi, T. Fujita, M. Asaeda, Nickel-doped silica membranes for separation of helium
413 from organic gas mixtures, Sep. Sci. Technol., 40 (2005) 225-238.
414 [20] M. Kanezashi, M. Asaeda, Hydrogen permeation characteristics and stability of Ni-doped silica
415 membranes in steam at high temperature, J. Membr. Sci. 271 (2006) 86-93.
416 [21] Y.F. Gu, P. Hacarlioglu, S.T. Oyama, Hydrothermally stable silica-alumina composite
417 membranes for hydrogen separation, J. Membr. Sci., 310 (2008) 28-37.
418 [22] K. Yoshida, Y. Hirano, H. Fujii, T. Tsuru, Hydrothermal stability and performance of silica-
419 zirconia membranes for hydrogen separation in hydrothermal conditions, J. Chem. Eng. Jap. 34
420 (2001) 523-530.
421 [23] Y. Gu, S.T. Oyama, Permeation properties and hydrothermal stability of silica-titania membranes
422 supported on porous alumina substrates, J. Membr. Sci. 345 (2009) 267-275.
423 [24] V. Boffa, D.H.A. Blank, J.E. ten Elshof, Hydrothermal stability of microporous silica and niobia–
424 silica membranes, J. Membr. Sci. 319 (2008) 256-263.

[25] A. Darmawan, J. Motuzas, S. Smart, A. Julbe, J.C. Diniz da Costa, Binary Iron Cobalt Oxide Silica Membrane for Gas Separation, J. Membr. Sci. 474(2015) 32–38.

[26] B. Ballinger, J. Motuzas, S. Smart, J.C. Diniz da Costa, Palladium Cobalt Binary Doping of Molecular Sieving Silica Membranes, J. Membr. Sci. 451(2014)185–191

[27] B. Ballinger, J. Motuzas, S. Smart, J.C. Diniz da Costa, Redox effect on binary lanthanum cobalt silica membranes with enhanced silicate formation, J. Membr. Sci. 489 (2015) 220–226.

[28] V Boffa, JE ten Elshof, AV Petukhov, DHA Blank, Microporous niobia–silica membrane with very low CO_2 permeability, ChemSusChem 1 (2008) 437-443.

[29] G. Ji, S. Smart, S.K. Bhatia, J.C. Diniz da Costa, Pore connectivity effect by the reduction of cobalt oxide silica membrane for gas permeation at high temperature, Sep. Purif. Technol. 154 (2015) 338–344.

[30] J.Y. Park, O. Levenspiel, The crackling core model for the reaction of solid particles, Chem. Eng. Sci., 30 (1975) 1207-1214.

[31] G. Uhde, U. Hoffmann, Noncatalytic gas-solid reactions: modelling of simultaneous reaction and formation of surface with a nonisothermal crackling core model, Chem. Eng. Sci., 52 (1997) 1045-1054.

[32] G. Olguin, C. Yacou, S. Smart, J.C. Diniz da Costa, Tailoring the oxidation state of cobalt through halide functionality in sol-gel silica, Sci. Rep. 3 (2013) 2449 doi:10.1038/srep02449.

[33] R.M. de Vos, W.F. Maier, H. Verweij, Hydrophobic silica membranes for gas separation, J. Membr. Sci. 158 (1999) 277-288.

[34] M.C. Duke, J.C. Diniz da Costa, D.D. Do, P.G. Gray, G.Q. Lu, Hydrothermally Robust Molecular Sieve Silica for Wet Gas Separation, Adv. Funct. Mater. 16 (2006) 1215-1220.

[35] G. Olguin, C. Yacou, S. Smart, J.C. Diniz da Costa, Influence of surfactant alkyl length in functionalizing sol-gel derived microporous cobalt oxide silica, RSC Adv. 4 (2014) 40181–40187.

[36] S.K. Sharma, P. Maheshwari, D. Dutta, K. Sudarshan, P.K. Pujari, Modification of microstructure of the surface and the bulk in ion-irradiated membrane studied using positron annihilation spectroscopy, Rad. Phys. Chem. 79 (2010). 1115-1119.

[37] F. Constantin, C. Barna, P. Mereuta, Positron annihilation spectroscopy studies of proton exchange membranes used in fuel cells, Polymers for Advanced Technologies 26 (2015) 1528-1530.

[38] C.-C. Hu, K.-R. Lee, R.-C. Ruaan, Y.C.Jean, J.-Y. Lai, Gas separation properties in cyclic olefin copolymer membrane studied by positron annihilation, sorption, and gas permeation J. Membr. Sci. 274 (2006), 192-199.

[39] X. Ma, H. Wang, H. Wang, J. O'Brien-Abraham, Y.S.Li, Pore structure characterization of supported polycrystalline zeolite membranes by positron annihilation spectroscopy, J. Membr. Sci. 477 (2015) 41-48.

[40] C.-Y. Tsai, S.-Y. Tam, Y. Lu, C.J. Brinker, Dual-layer asymmetric microporous silica membranes, J. Membr. Sci. 169 (2000) 255-268.

[41] H. Gharibi, B.M. Razavizadeh, A.A. Rafati, Electrochemical studies associated with the micellization of dodecyltrimethyl ammonium bromide (DOTAB) in aqueous solutions of ethanol and l-propanol, Coll. Surf. A –Physicochem. Eng. Asp. 136 (1998) 123-132.

[42] J.B. Huang, M. Mao, B.Y. Zhu, The surface physico-chemical properties of surfactants in ethanol-water mixtures, Coll. Surf. A –Physicochem. Eng. Asp. 155 (1999) 339-348.

[43] E. Fuguet, C. Ràfols, M. Rosés, E. Bosch, Critical micelle concentration of surfactants in aqueous buffered and unbuffered systems, Analytica Chim. Acta 548 (2005) 95-100.

[44] A. Wagner, W. Anwand, A.G. Attallah, G. Dornberg, M. Elsayed, D. Enke, A.E.M. Hussein, R. Krause-Rehberg, M.O. Liedke, K. Potzger, T.T. Trinh, Positron annihilation lifetime spectroscopy at a superconducting electron Accelerator, J. Phys.: Conf. Ser. 791 (2017) 012004.

[45] A. Wagner, M. Butterling, M.O. Liedke, K. Potzger, R. Krause-Rehberg, Positron annihilation lifetime and Doppler broadening spectroscopy at the ELBE facility, AIP Conf. Proc. 1970 (2018) 040003.

[46] M.J. Puska, R. M. Nieminen, Theory of positrons in solids and on solid surfaces, Rev. Modern Phys. 66 (1994) 841–97.

[47] K. Wada, T. Hyodo, A simple shape-free model for pore-size estimation with positron annihilation lifetime spectroscopy, J. Phys.: Conf. Ser. 443 (2013) 012003.

[48] A. Shukla, M. Peter, L. Hoffmann, Analysis of positron lifetime spectra using quantified maximum entropy and a general linear filter, Nucl. Instrum. Methods Phys. Res. A 335 (1993) 310-317.

[49] M.C. Duke, S.J. Pas, A.J. Hill, Y.S. Lin, J.C. Diniz da Costa, Exposing the molecular sieving architecture of amorphous silica using positron annihilation spectroscopy, Adv. Funct. Mater. 18 (2008) 3818-3826.

[50] D. Uhlmann, S. Liu, B. P. Ladewig, J. C. Diniz da Costa, Cobalt-doped silica membranes for gas separation, J. Membr. Sci. 326 (2009) 316–321.

[51] R.M. de Vos, H. Verweij, Improved performance of silica membranes for gas separation, J. Membr. Sci. 143 (1998) 37-51.

[52] J.C. Diniz da Costa, G.Q. Lu, V. Rudolph, Y.S. Lin, Novel molecular sieve silica (MSS) membranes: characterisation and permeation of single-step and two-step sol–gel membranes, J. Membr. Sci. 198 (2002) 9-21.

[53] R.S.A. de Lange, K. Keizer, A.J. Burggraaf, Analysis and theory of gas transport in microporous sol-gel derived ceramic membranes, J. Membr. Sci. 104 (1995) 81-100.

[54] R. M. Barrer, Porous Crystal Membranes, J. Chem. Soc. Faraday Trans. 86 (1990)1123-1130.

[55] W.J. Bakker, L.J.P. van den Broeke, F. Kapteijn, J. A. Moulijn, Temperature dependence of one-component permeation through a silicalite-1 membrane, AIChE J. 43 (1997) 2203-2214.

[56] C. J. Brinker, G. W. Scherer, Sol Gel Science: the physics and chemistry of the sol gel processing, (1990) Academic Press, San Diego, USA.

[57] C.J. Brinker, A.J. Hurd, K.J. Ward, Fundamentals of sol-gel thin-film formation in: Ultrastructure Processing of Advanced Ceramics, eds J. D. Mackenzie, D. R. Ulrich, Wiley, New York (1988) 223-253.

[58] D.L. Meixner, P.N. Dyer, Characterisation of the transport properties of microporous inorganic membranes, J. Membr. Sci. 140 (1998) 81-95.

Declaration of interests

☒ The authors declare that they have no known competing financial interests or personal relationships that could have appeared to influence the work reported in this paper.

☐The authors declare the following financial interests/personal relationships which may be considered as potential competing interests:

Surfactant functionalized cobalt silica membranes – gas permeation and thin film positron annihilation lifetime spectroscopy characterisation

Gianni Olguin[1,2*], Christelle Yacou[1,3], J. Motuzas[1], Maik Butterling[4], Wilhelm A. Meulenberg[5], Simon Smart[1], João C. Diniz da Costa[1,6,7*]

Author Statement

G. Olguin: conceptualisation, investigation, validation, analysis, writing, review & editing.

C. Yacou: membrane analysis & supervision.

J. Motuzas: SEM investigation & analysis.

M. Butterling: PALS investigation, validation, analysis, writing, review & editing.

W.A. Meulenberg: conceptualisation, analysis, supervision & funding acquisition.

S. Smart: conceptualisation, supervision, analysis, writing, review & editing & funding acquisition.

J.C. Diniz da Costa: conceptualisation, supervision, analysis, writing, review & editing, project administration & funding acquisition.

Surfactant functionalized cobalt silica membranes – gas permeation and thin film positron annihilation lifetime spectroscopy characterisation

Gianni Olguin[1,2*], Christelle Yacou[1,3], J. Motuzas[1], Maik Butterling[4], Wilhelm A. Meulenberg[5], Simon Smart[1], João C. Diniz da Costa[1,6,7*]

[1]The University of Queensland, FIM[2]Lab – Functional Interfacial Membranes and Materials Laboratory, School of Chemical Engineering, Brisbane Qld 4072, Australia.

[2]Pontificia Universidad Católica de Valparaíso, Escuela de Ingeniería Química, Valparaíso, Chile.

[3] Laboratory COVACHIM-M2E, EA 3592, Université des Antilles, BP 250, 97157 Pointe-à-Pitre, Guadeloupe, France.

[4]Helmholtz-Zentrum Dresden - Rossendorf, Institute of Radiation Physics, Bautzner Landstraße 400, 01328 Dresden, Germany

[5]Forschungszentrum Jülich, Institute of Energy and Climate Research (IEK - 1), Wilhelm - Johnen - Strasse, 52425 Jülich, Germany

[6]LAQV-REQUIMTE, (Bio)Chemical Process Engineering, Department of Chemistry, Faculty of Science and Technology, Universidade NOVA de Lisboa, 2829-516 Caparica, Portugal.

[7]iBET – Instituto de Biologia Experimental e Tecnológica, 2781-901 Oeiras, Portugal.

Abstract

This work investigates the use of positron annihilation lifetime spectroscopy (PALS) for the in-situ structural characterisation of silica derived thin film membranes. By using a quantified maximum entropy method, PALS allowed for the measurement of porous volumetric fraction and a pore size distribution depth profile. PALS measurements were carried out on a series of silica derived membranes where alumina supports were coated with four layers of cationic HTBA surfactant cobalt silica sols wherein the surfactant / cobalt molar ratio loading varied from 0 to 3. PALS results showed

that the coated layers adjacent to the porous alumina substrate were characterised by micropores and broad mesopores, a clear indication that the porosity of the substrate affected the pore size at the substrate and thin film interface. The last coated layer resulted in narrow micropores with a trimodal pore size distribution of 0.5-0.6 nm, ~1nm and ~3nm. This was attributed to the surface smoothness conferred by three previous coated layers. The increase in the surfactant loading led to an increase in the pore fraction of thin films as ascertained by PALS. These results correlated quite well with the gas permeation and selectivity results. Higher surfactant loadings resulted in an increase is gas permeation and reduction of He/CO_2 selectivity from 91.5 to 3.8. PALS proved to be a powerful tool characterisation of the structural features of microporous thin films.

Keywords: silica membranes; surfactant; pore size; thin film; gas permeation.

1. Introduction

Gas separation is a major chemical engineering process, important to a wide variety of industries, where removal of undesirable species or concentration of products is desirable. There are many processes used for gas separation such as (i) cryogenics involving very low temperatures and changing phase from gas to liquid [1, 2]; (ii) adsorption processes requiring gas cooling to room temperatures to take advantage of sorbents sorption capacities at low temperatures [3, 4]; (iii) absorption processes where gases react with solvents thus requiring a downstream desorbing processing [5, 6]; and (iv) membranes which can separate gases without phase change [7]. As many industrial gases are generated at high temperatures and high pressures the use of inorganic membranes, which are chemically and thermally stable, is attractive [8]; particularly palladium alloys [9] and molecular sieving silica [10-12]. Of particular attention cobalt oxide silica membranes have been scaled up with proven performance for 2000 hours operation and reaching very high H_2/CO_2 permselectivities of 500 [13].

Metal oxide silica membranes are synthesised from a silica sol-gel method using hydrated metal nitrates which are oxidised during synthesis. Embedding cobalt oxide into silica films conferred functionalities otherwise not available in pure silica membranes, such as improvements for wet gas separation [14-16], although the mechanism of protection was not clear. More recently, work by Liu and co-workers [17, 18] reported that the Co^{3+} coordination with Si increased hydro-stability, whilst hydrolytic attack was severe on membranes containing a higher concentration of Co^{2+} coordinated with Si. The literature contains a multitude of metal oxides incorporated into silica thin films from the initial examples of oxides of nickel [19, 20], to aluminium [21], zirconium [22], titanium [23], niobium [24], and more recently binary oxides of cobalt with iron [25], palladium [26] and lanthanum [27].

Different oxides also confer different functionalities to the resultant membranes. For instance, niobium oxide silica membranes provided relatively good N_2/CO_2 permselectivity of ~8 [28], higher than any previous silica membranes of values below 2-3. In the case of adding lanthanum to a CoSi membrane, it allowed the formation of silicates which enhanced the thermal stability of the pore sizes below 3Å under reduction and oxidation cycles [26]. In another case, Ji et al. [29] demonstrated that pore connectivity of CoSi membranes increased as the membranes were reduced using a H_2 rich atmosphere at high temperatures. This was attributed to the effect of the gas to solid reaction of H_2 to the cobalt oxide particle (Co_3O_4) which was reduced to CoO. During reduction, cobalt oxide particles breaks into small particles, known as the crackling core model [30, 31], and formed additional permeation channels.

In the pursuit of additional functionalities, Olguin and co-workers [32] reported that the oxidation state of cobalt oxide could be tailored by the halide functionality of surfactants in silica gels. Whilst this work focused on xerogels, surfactants and carbon templates have been previously used for the preparation of silica membranes. For instance, Verweij and co-workers [33] carbonised a ligand

methyl group to silica precursors which improved the hydro-stability of the silica membranes. Duke et al. [34] carbonised surfactants embedded in silica xerogels and showed that the carbon moieties were like barriers opposing the movement of unstrained silica groups, thus avoiding densification under hydrothermal conditions. In a further work, Olguin et al. [35] showed that the length of the alkyl group and the surfactant concentration influenced the porous structural formation of cobalt oxide silica xerogels.

The published works on the effect of surfactants on CoSi has been limited to xerogel studies, whilst membranes have yet to be fully reported. This is an important point as the chemical and physical principles that control the silica structural formation are, in theory, the same for both bulk xerogels and thin films. However, the latter undergoes fast gelation and evaporation of solvents (i.e. water), and the final structure of surfactant functionalised CoSi thin films may differ from that of bulk xerogel. A characterisation technique to study thin films in membranes is positron annihilation spectroscopy (PALS) that has been reported for polymeric membranes [36-38], and crystalline inorganic (i.e., zeolite) membrane [39]. In the case of amorphous silica membranes, publications on in situ characterisation of silica thin films supported by substrates is even more limited as in principle the silica sol-gel solution slightly penetrates into the pores of interlayer due to capillary forces during film coating.

Therefore, this work investigates two important aspects of silica derived membranes. The first investigation focuses on determining the pore structure of supported thin films using PALS. The second investigation studies the performance of surfactant functionalised CoSi membranes for gas separation. Hexyl trimethyl ammonium bromide (HTAB) was chosen as the functional surfactant in view of its effect in the oxidation state of CoSi xerogels [35]. A series of membranes were prepared via a sol-gel synthesis method, where the concentration of HTAB was varied. Single gas permeation of He, H_2, N_2 and CO_2 was performed for each of the prepared membranes at different testing

temperatures in the range 200-500 °C. This work is particularly interested in understanding how the surfactant functionalities on CoSi membranes in terms of porosity and pore sizes as determined by PALS can affect gas transport phenomena and membrane performance.

2. Experimental

Cobalt silica (CoSi) coating solutions were synthesised via a sol-gel method. Cobalt nitrate hexahydrate ($Co(NO_3)_2.6H_2O$) was dissolved in 30 %vol hydrogen peroxide (H_2O_2) in order to keep the pH stable around 3.0 and then diluted in an excess of ethanol. Subsequently, the solution was cooled to 0 °C, followed by a slow drop-wise addition of tetraethyl orthosilicate (TEOS). The final TEOS : H_2O : H_2O_2 : EtOH : $Co(NO_3)_2.6H_2O$ molar ratios was 4 : 45.5 : 9 : 256 : 1, which was moderately stirred in an ice-bath at 0 °C for three hours. The preparation of surfactant cobalt silica followed the same procedure, except for the addition of hexyl trimethyl ammonium bromide (HTAB) after the ice-bath treatment. Surfactant concentration was varied based on the surfactant/cobalt molar ratio (*x*) 0 to 3 and the resultant sols were named as CoSi-S(x). The HTAB concentration variation aimed at varying the pore size and pore volume of the resultant CoSi membranes based on homologue xerogels published elsewhere [32, 35]. The solubility of surfactant was achieved by keeping the concentration below the critical micelle concentration (CMC) point, taking into account the surfactant type [40], solvent nature [41, 42] and counter ion presence [43]. The HTAB concentration in our surfactant-cobalt silica sol was varied from 0 (*x=0*) to 180 mM (*x=3*) below the CMC of 2000 mM.

Membranes were prepared by dip coating four active silica layers on outer shell of a commercial alumina substrate (Energy Research Centre of the Netherlands). The dimensions of the tubes were 14 mm external diameter with 2 mm thick wall, a length of 200 mm. The tubes contained an asymmetric structure, with α-alumina substrate followed by small α-alumina particle interlayers, and thin γ-alumina interlayers with 4nm pore sizes. A conventional dip coater was used to coat silica layers through a constant immersion and withdrawal speed of 10 cm min^{-1} and dwell time of 1 min. Each

silica layer was subsequently calcined in an electric furnace at 630 °C under air atmosphere, a ramping rate of 1 °C min^{-1} and a dwell time of 2.5 hr. Under these calcination temperatures, the HTBA is fully burnt off [32], resulting in the formation of a surfactant free CoSi membranes.

The performance of each membrane was assessed by single gas permeance of He, H_2, N_2 and CO_2 at four different operation temperatures (200, 300, 400 and 500 °C) in a custom permeation rig (see Fig. 1). The permeate stream was kept at atmospheric pressure while feed pressure was set constant at 400 kPa. A series of leaking tests were run each time before membrane testing, to ensure that any problems associated with seal failure or membrane fractures were not present. The leaking tests involved checking gas leaks in valves and connections in the gas permeation rig and membrane module. The membrane was sealed using graphite seals developed by Yacou and co-workers [13], that allows gas permeation testing at high temperatures without sheering ceramic tubes. The membranes with high gas permselectivities were considered gas leak free and defect free.

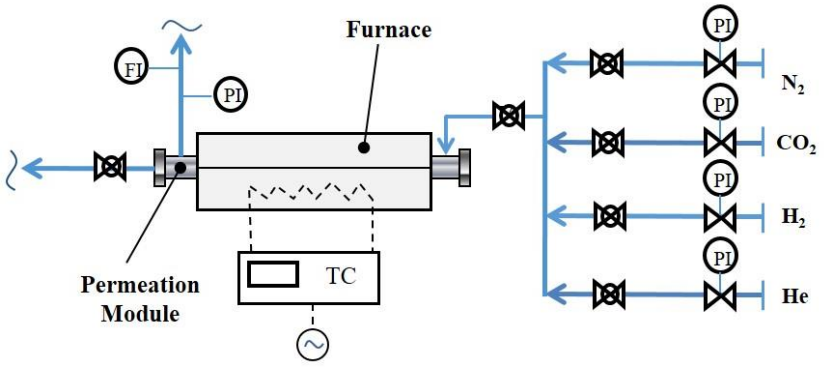

Fig. 1 - Single gas permeation rig: pressure regulator (PI), flow rotameter (FI), temperature controller (TC).

Positron annihilation lifetime spectroscopy (PALS) experimental set up required a flat and homogeneous surface for thin film analysis since the probing positron beam has a diameter of around 5 mm. Therefore, PALS was carried on flat alumina supports made of α-alumina substrate and a thin layer of γ-alumina (supplied by Pervatech) with 80 nm pore size. Each support was dip coated with

4 active silica layers on a custom coater, taking into consideration similar parameters to the tubular membranes. The calcination procedure for each layer was the same as for the tube membranes. Samples of the latter were analysed by a field emission scanning electron microscope (JEOL Model JSM-7001F) to observe their morphological features. The analysis was performed using a 5kV acceleration voltage and a distance of 10 mm.

The PALS experiments were performed at the mono-energetic positron source (MePS) beamline, which is one of the end stations of the radiation source ELBE (Electron Linac for beams with high Brilliance and low Emittance) at HZDR (Germany) [44, 45], using positrons produced from high-energy bremsstrahlung of the 30 MeV electron source ELBE. The PALS spectra were recorded using a fast $CeBr_3$ scintillator detector coupled to a Hamamatsu R13089-100 PMT. After implantation into a solid, positrons lose their kinetic energy due to thermalization and, after a short period of diffusion, annihilate in delocalized lattice sites or localize in vacancy-like defects and pores, emitting usually two anti-collinear 511 keV gamma photons after annihilation with the encountered electrons. The implantation profile can be calculated via a Makhovian distribution [46] (see Appendix Fig. A1). A mean positron implantation depth can be approximated by a simple material density-dependent, Makhovian positron stopping profile formula [42]: $\langle z \rangle = 36/\rho \cdot E_p^{1.62}$, with the material density, ρ and positron implantation energy, E_p. Positron implantation energy was varied from 0.5 to 12 keV providing an approximated depth profile between 0 and 100 nm.

Positron lifetime components were obtained through a quantified maximum entropy method. The porous volumetric fraction of surfactant functionalised silica layers was calculated averaging the shortest lifetime component (related with annihilation within material) along with silica thickness. The pore size distribution (PSD) depth profile is based on the positron energy which changes with the implantation depth (see Appendix Fig. A1), and allows the pore size of the sub-layers to be analysed and determined. The collected data are known as PALS lifetime distribution, given by the

annihilation versus lifetime value for each implantation depth. The PALS lifetime distribution represents multiple cavities sizes in the surfactant functionalised silica membrane, thus requiring deconvolution to determine the pore size of the cavities (see Appendix Fig. A2). Deconvolution is carried out using non-standard gaussian peaks to get lifetime components (τ_5, τ_4, τ_3…) which can be translated into pore sizes according to a simple shape-free model based on the extended Tao-Eldrup model for pore size determination from PALS [47] (see Appendix Fig. A3). For each spectrum $3x10^6$ counts were recorded at a rate of 3600 counts per second, for positron implantation energies from 0.5 keV to 12 keV (Appendix Fig. A4). Positron lifetime components were then obtained based on the maximum entropy method using the MELT (maximum entropy lifetime analysis) software package [48]. In contrast to a discrete lifetime analysis using multi-exponential decay functions, a MELT analysis allows to extract pore size distributions rather than only discrete pore sizes as detailed in the Appendix.

3. Results

3.1 Characterisation

Representative SEM images of the as-prepared membrane are depicted in Fig. 2. The cross-section is composed of a surfactant functionalised cobalt silica top layer coated on a γ-Al_2O_3 interlayer. The latter was coated on a macroporous α-Al_2O_3 substrate characterised by a coarse surface containing large particles. The interlayer is required to reduce the roughness of the substrate surface to enable coating of the top layer. The top layer has a homogeneous surface coverage in all directions with a thickness of ~120 nm. A total of four surfactant cobalt layers were coated on the substrate, suggesting that each coated layer resulted in a thickness of ~30 nm upon calcination.

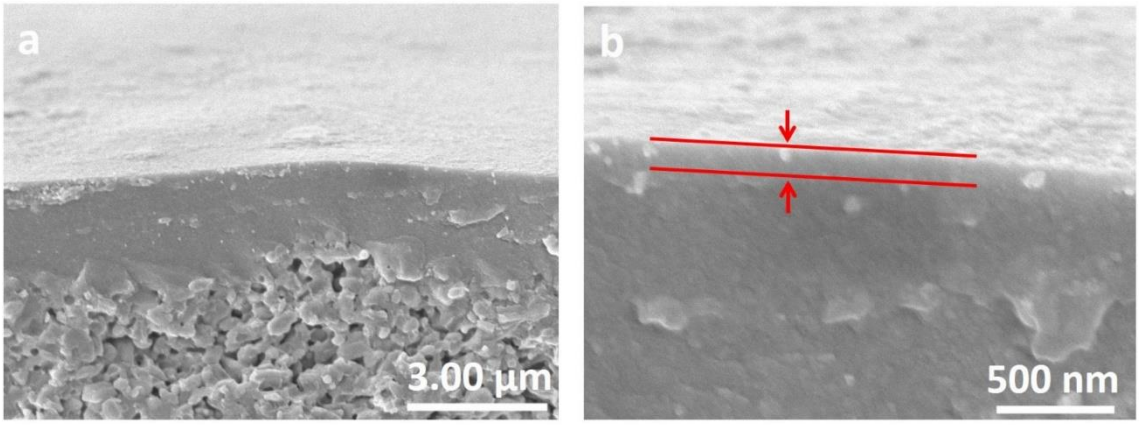

Fig. 2. Representative SEM image of surfactant functionalised cobalt silica membrane.

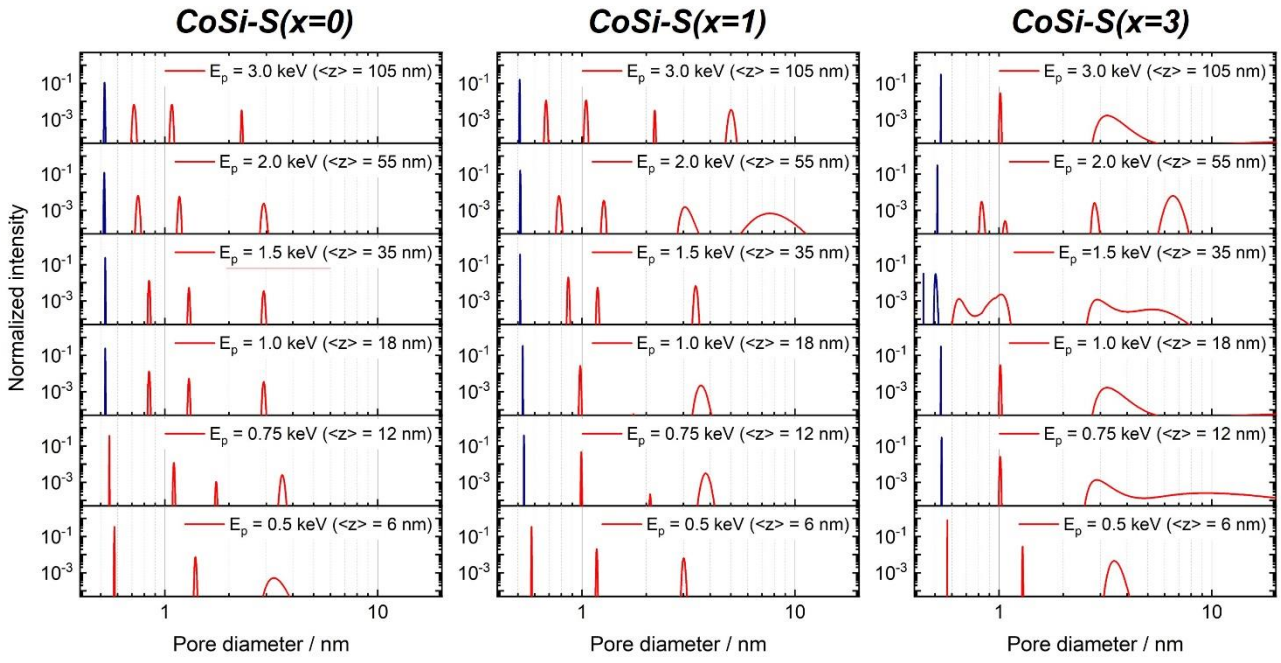

Fig. 3. Positron pore size distribution for different positron implantation energies E_p for a surfactant functionalised CoSi membranes. The mean implantation depths <z> are calculated from the Makhovian stopping profiles using $\langle z \rangle = 36/\rho \cdot E_p^{1.62}$. Usually, positrons are implanted in a much wider depth range (see appendix Fig. A1), therefore the given values are just a rough estimation. The blue narrow peak around 0.5 nm is not a signal from annihilation in pores but from free positrons annihilating in the matrix material. Although this lifetime component is not related to a pore, the peak is shown here in the figure for comparing free positron annihilation and annihilation in pores.

196

197 Fig. 3 displays PSD profiles along the depth of the surfactant functionalised cobalt silica membranes.
198 The PSD profile shows a relative abundance of pore sizes at each depth, grouped as micropores ($d_p <$
199 2 nm) and mesopores ($2 \leq d_p \leq 50$ nm). The presence of a tri-modal PSD at depths up to 18 nm, are
200 in line with the PALS work pioneered by Duke et al. [49] for silica powders. Importantly though, the
201 top portion of fourth and final coated layer (from 0 to ~ 30 nm) for membranes *x=0* and *x=1* showed
202 high intensity peaks at $d_p < 2$ nm as compared to larger implantation depths, reflecting a shift to
203 micropore PSD. This is attributed to the surface smoothness of the previous coated and calcined
204 surfactant functionalised silica layers. It strongly indicates that four layers were sufficient to produce
205 a defect free thin film. The membrane *x=3* exhibited a higher contribution of peaks at $d_p > 2$ nm, a
206 clear indication of the formation of mesopores. This is attributed to higher concentration of HTAB
207 that are burnt off upon calcination, contributing to pore size enlargement.
208

209 Beyond a film depth of >35nm (for the 2nd and 3rd coated layers to be precise) the intensity of the
210 peaks associated with mesopores broadens for membranes *x=0* and *x=1*, confirming the incorporation
211 of more mesopores into the CoSi thin film layers. The increase in the contribution of mesopores may
212 be associated with morphological effects which stem from the underlying larger pores in the substrate.
213 However, the drying and calcination process is clearly complex as the first coated layer at a PALS
214 depth of 105 nm actually showed a lower mesopore contribution than the 2nd and 3rd layers (at 55nm
215 and 35nm respectively). Similarly, the membrane *x=3* also displayed a reduction of the contribution
216 of mesopores. In this case, the PSD may be associated with the intrusion of the surfactant cobalt silica
217 sol into the mesopores of the interlayer.
218

219 The determination of the PSD depth profile also allowed for the calculation of the positron porosity
220 fraction as displayed in Fig. 4. The porosity fraction is the fraction of all positrons annihilating in

221 micro- and mesopores. Remaining positrons are annihilating as free positrons (see blue peak in Fig.
222 3). Fig. 4 displays the pore values as PALS porosity fraction and pore volumes determined from
223 nitrogen sorption isotherms. It is observed that by increasing the surfactant ratio (*x*) used to prepare
224 the functionalised surfactant cobalt silica thin films, the positron porosity fraction likewise increased.
225 The surfactant molecules act as templates or free-volume spaces embedded into the cobalt silica
226 matrix. Upon calcination in air, the surfactant is fully burnt-out at 530 and 550 C [32] for membranes
227 *x=1*and *x=3*, respectively. By raising the calcination temperature further, the porous cobalt silica thin
228 film densifies, and the positron porosity fraction was linear with respect to the surfactant ratio.

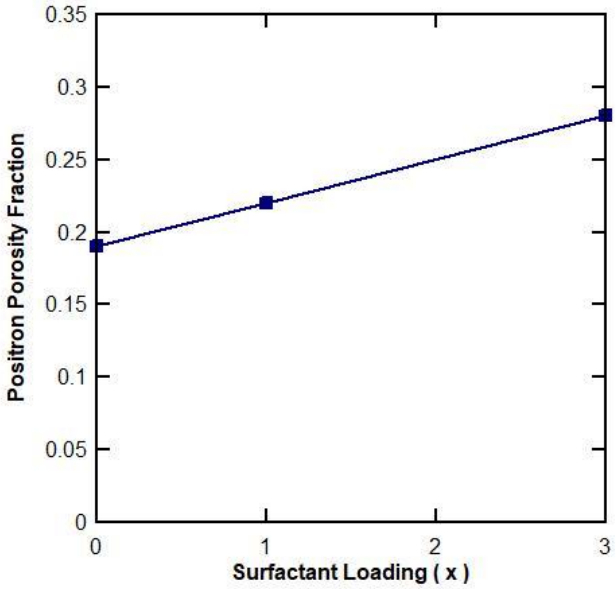

229

230 Fig. 4. Positron porosity fraction as a function of the surfactant ratio (*x*) used to prepare the
231 functionalised surfactant cobalt silica membranes.

232 **3.2 Gas permeation**

233 Fig. 5 shows the single gas permeance of He, H_2, N_2 and CO_2 gases at various temperatures for three
234 tested membranes. The CoSi (*x*=0) membrane, with no surfactant loading, follows the traditional
235 temperature dependent gas transport as reported elsewhere for cobalt silica membranes [13, 50] and
236 silica membranes [51, 52] based on the transport of gases in microporous materials [53]. This
237 membrane is characterised by the permeance of the smaller gases, He (d_k=2.6 Å) and H_2 (d_k=2.89 Å),

increasing with temperature, whilst the permeance of the larger gases, CO_2 (d_k=3.3 Å) and N_2 (d_k=3.64 Å), decreased with temperature. Similar behaviour was observed for the SCoSi (x=1), though the larger gases showed almost no decline in permeance as the testing temperature was raised. By adding more surfactant as SCoSi (x=3) membrane, the single gas transport behaviour changed. For instance, gas permeance in this x=3 membrane remains steady as a function of the temperature, within experimental error of ±8%. Further, the single gas permeation curves for the smaller and larger gases are much closer, and not as distanced as for the lower surfactant loaded membranes (x=0 and 1). The results in Fig. 5 strongly suggest that surfactant loading is conferring morphological changes to the final structure of the cobalt oxide silica membranes.

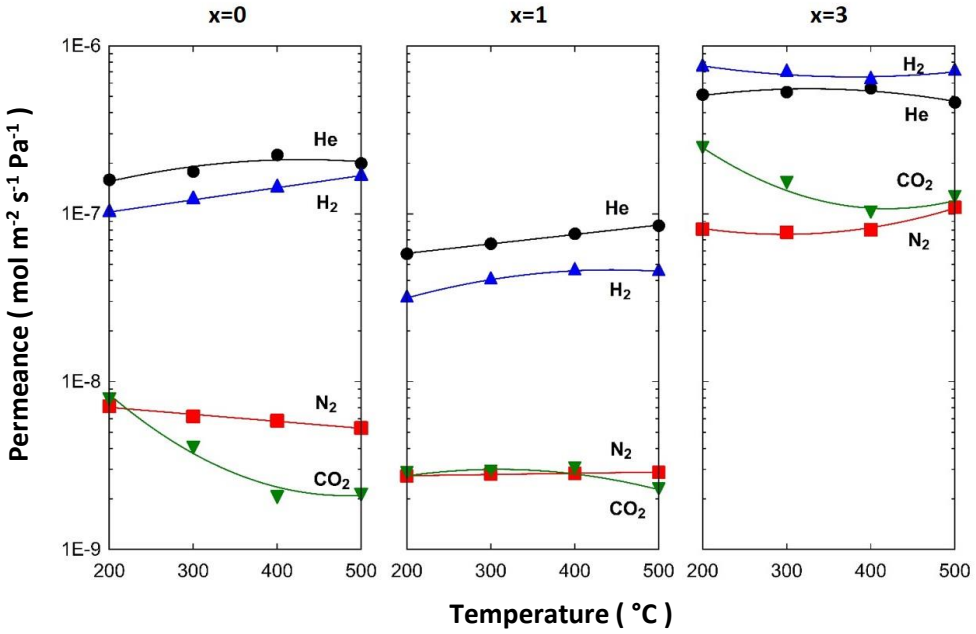

Fig. 5. Single gas permeance (±8%) as a function of temperature for membranes with varied surfactant loading (x).

The temperature dependent transport observed in Fig. 5 is also known as activated transport based on Barrer's model [54] for gas diffusion via microporous structures. Fig. 6 shows the apparent energy of activation (E_{act}) for H_2 and N_2 as a function of surfactant loading. The E_{act} was calculated from the Arrhenius plot of the permeance of for H_2 and N_2. In principle, E_{act} gives a good indication of pore

size changes provided that gas permeation follows activated transport. For instance, smaller micropores are characterised by higher He and lower N_2 E_{act} values. This is clearly observed for membranes *x=0 and 1*. However, membranes *x= 3* shows that a convergence of both E_{act} values, given a clear indication of increased pore sizes. This shows a departure from activated transport to Knudsen diffusion, a characteristic of pore size change from micropore to mesopore. These results correlated well with the positron PSD in Fig. 3.

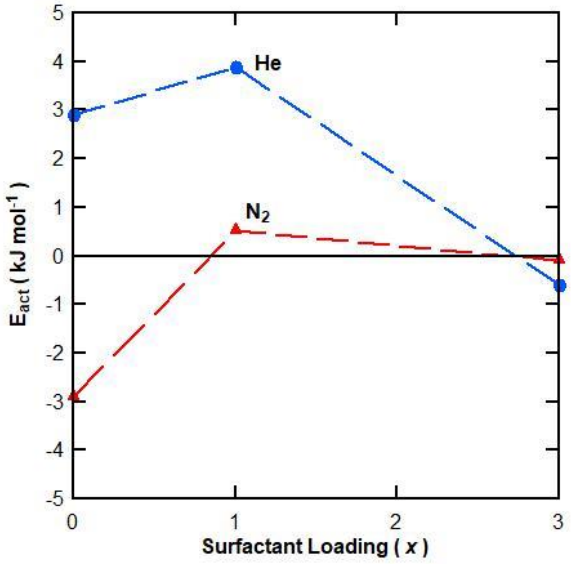

Fig. 6. Apparent energy of activation (E_{act}) for H_2 and N_2

Fig. 7a displays the permselectivity of several gas pairs at 500 ^oC. The permselectivity was determined from the ratio of the permeance of each gas pair. It is interesting to observe that membrane *x=0* showed higher He/CO_2 (91.5) and H_2/CO_2 (77.0) as compared to He/N_2 (37.7) and H_2/N_2 (31.8). Considering that the kinetic diameter of CO_2 (d_k=*3.3 Å*) is smaller than that N_2 (d_k=*3.64 Å*), the permselectivity should be higher for gas pairs containing N_2 instead of CO_2 for molecular sieve membranes. Nevertheless, this is attributed to the adsorption effect in ultramicroporous silica membranes such as membrane *x=0*. The isostheric heat of adsorption Q_{st} in CoSi membranes for CO_2 (Q_{st} = *22.7 kJ mol^{-1}*) [29] is higher than N_2 (Q_{st} = *5 kJ mol^{-1}*) [50]. Q_{st} represents an energy barrier

and higher values leads to the reduction of permeance as a function of temperature as observed in Fig. 5 for membrane x=0. As the pore sizes increase, adsorption becomes less prevalent and permselectivity decreases as observed for membrane x=1. In the case of membrane *x=3*, the permselectivity for the gas pairs converged to similar values, confirming the enlargement of pore sizes as observed in the positron PSD (Fig. 3).

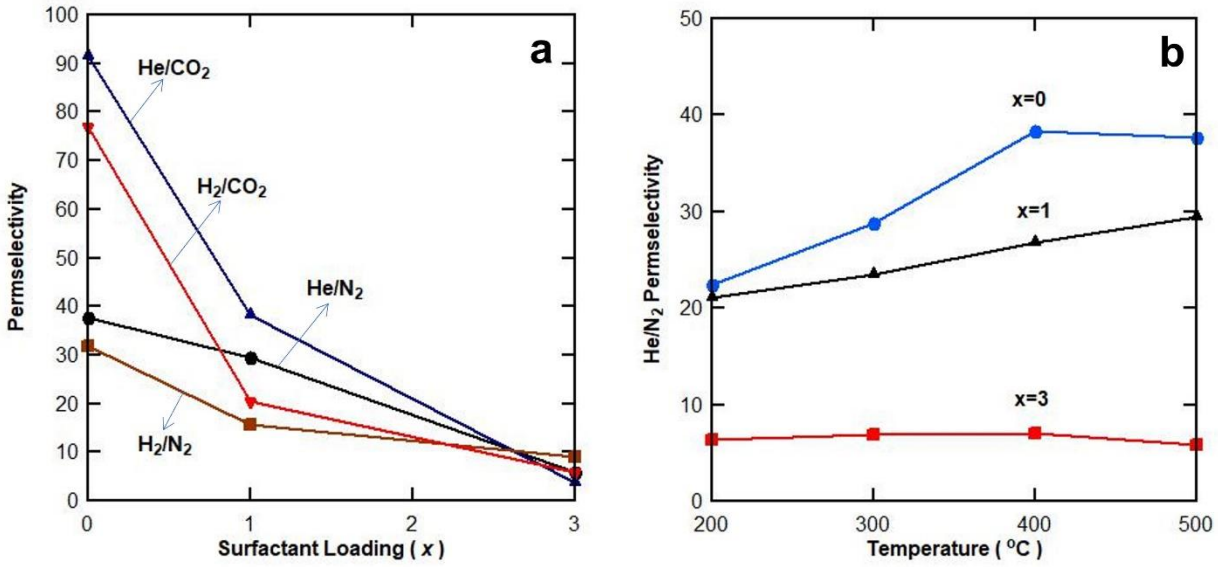

Fig. 7. (a) Permselectivity of gas pairs at 500 °C as a function of membrane surfactant loading, and (b) He/N_2 permselectivity for all membranes as a function of temperature.

Fig. 7b shows the He/N_2 permselectivity for all membranes as a function of temperature. Helium is a non-adsorbable gas [55] under the testing conditions in this work. The increase in He/N_2 as a function of temperature reflects the effect of N_2 adsorption for membranes *x=0 and 1*. The He/N_2 permselectivity is low for *x=3*, around 6.5 and remained almost constant. As the ideal Knudsen selectivity of He/N_2 is 2.6, the low permselectivity strongly suggest that the transport phenomena behaviour changed from molecular sieving for SCoSi (*x=0 and 1*), to Knudsen transport for SCoSi (*x=3*). This is in line with the pore size broadening, where silica apertures control the passage of

gases. This result correlates well with the positron PSD (Fig. 3) for membrane *x=3*, evidenced by the contribution of mesopores in the CoSi thin films.

To understand further the morphological features of the membranes in this work, the average pore sizes calculated from PALS SCoSi thin film measurements (Fig. 3) are compared against those obtained for homologue xerogels from conventional N_2 sorption. Fig. 8 shows the He/N_2 at 500 °C plotted as function of pore sizes for PALS and N_2 sorption. It is well known that the pore size in microporous membranes control the separation of gases of different kinetic diameters. This is true for both measurements as He/N_2 permselectvities decrease as pore sizes increase. However, it is observed in Fig. 8 that pore sizes obtained from N_2 sorption display small variations from 2.1 to 2.4 nm as the surfactant load was raised from x=0 to 3, respectively. PALS measurements showed a better resolution as pore sizes varied from 1.2 to 3 nm in the same range of surfactant loading.

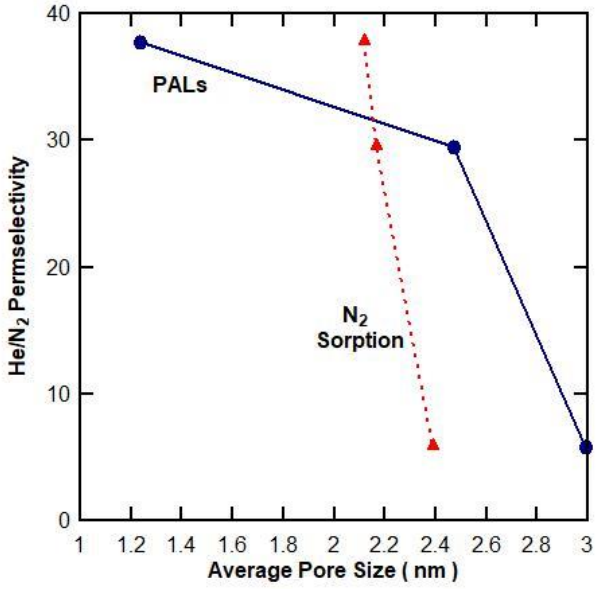

Fig. 8. He/N_2 permeance at 500 °C as a function of average pores based on PALs (blue circles-solid line) for membranes calcined at 630 °C and N_2 sorption for xerogels calcined at 600 °C [32] (red triangles-dashed line). Lines are provided to better identify the two data series.

Morphological differences stemming from PALS and N_2 sorption measurements are observed further in Fig. 9. In principle, if pore fraction or pore volume increases, then the trend is for permeation to increase too as there is less resistance for gas transport through the membrane. Indeed, this is the case for the PALS measurements though the initial point is slightly scattered but within the permeation experimental error of 8%. In the case of pore volumes from N_2 sorption, the permeation results buck this trend in this work. Both He and N_2 permeance have similar pore volumes for the surfactant sols x=1 and 3, but the differences in permeance results are 5.5 and 33 times, respectively.

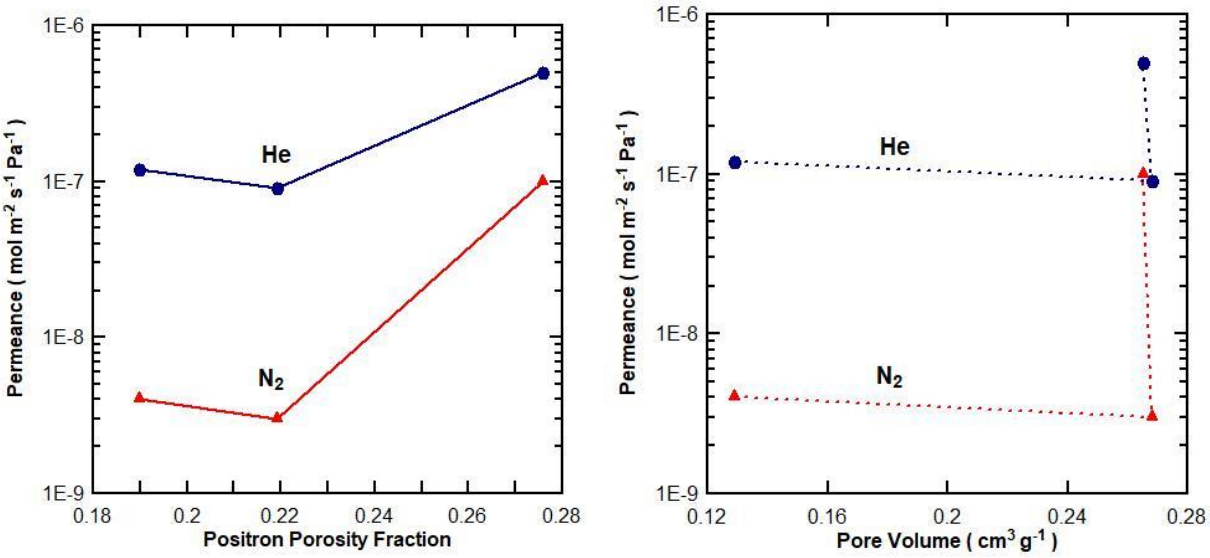

Fig. 9. He and N_2 permeance at 500 °C as a function of (a) positron porosity faction determined from PALS for membranes calcined at 630 °C and (b) pore volumes determined from N_2 sorption isotherms for xerogels calcined at 600 °C [32]. Lines are provided to better identify the two data series.

Figs. 8 and 9 clearly show that PALS measurements provide better precision for thin films based on permeation properties. Although the underlying physics and chemistry that govern silica growth and gelation are essentially the same for films as bulk gels, other factors influence structural evolution in films [56]. For instance, the properties of a deposited thin film may be quite different due to non-equivalent gelation and drying conditions [57, 58]. The PALS results in this work clearly show that the morphological features of silica derived thin films and xerogels are different, thus addressing

these important and valid points raised by Brinker and co-workers [56, 57] and Meixner and Dyer [58] over two decades ago.

4 Conclusions

PALS characterisation of surfactant loaded CoSi thin films showed a higher contribution of micropore formation on the top layer, to a depth of ~12 nm. The PSD tended to show an increased fraction of micropores and mesopores at higher penetration depths (i.e., closer to the porous alumina interlayer), suggesting the substrate porosity affected the pore formation in the adjacent membrane layers. Gas permeation testing confirmed that the incorporation of a cationic surfactant as a secondary dopant component on cobalt containing silica altered separation performance. High loads of surfactant increased gas permeance resulting in reduced selectivities, a demonstration of pore size increase. The permeation and selectivity results are consistent with the PALS measurements where the porosity fraction and pore sizes also increased with the surfactant load of the prepared membranes. PALS measurement of thin films structural features is powerful characterisation tool that showed strong correlations the transport properties of the surfactant CoSi membranes.

Acknowledgment

The authors would like to acknowledge funding support from the Australian Research Council through Discovery Project Grant DP110101185. G. Olguin acknowledges funding support from the bicentenary scholarship program from the Chilean Government and Jan S. Eiberger from the Forschungszentrum Jülich in Germany regarding discussions on PALS. J. C. Diniz da Costa gratefully thank the support given by the Australian Research Council Future Fellowship (FT130100405) program and the grant as invited Professor funded by the Associate Laboratory for Green Chemistry – LAQV, financed by the National Portuguese funds from FCT/MCTES (UIDB/50006/2020).

Competing interests

The authors declare no competing interests.

Appendix

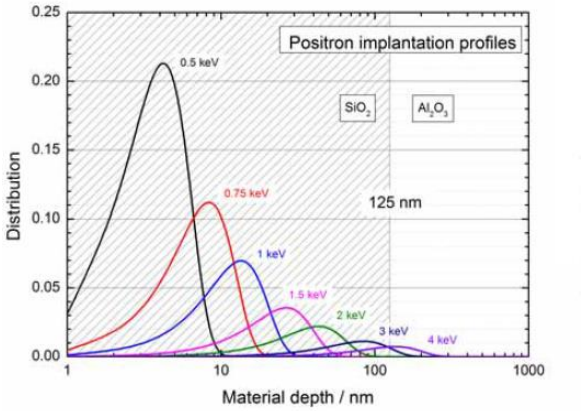

Fig. A1. Implantation depth profile versus positron energy for the case of SiO_2 on Al_2O_3 [42].

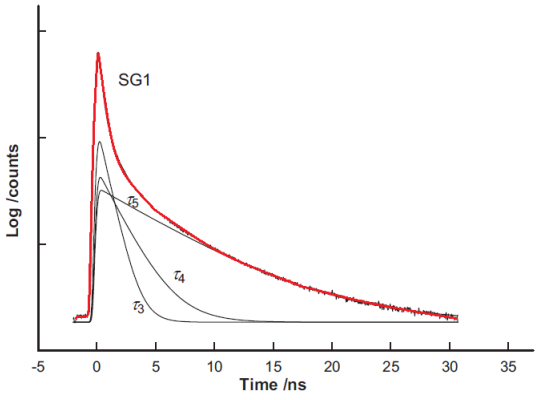

Fig. A2. Deconvolution of the positron annihilation lifetime spectrum of a surfactant functionalised cobalt silica membrane (*x=1*) [49].

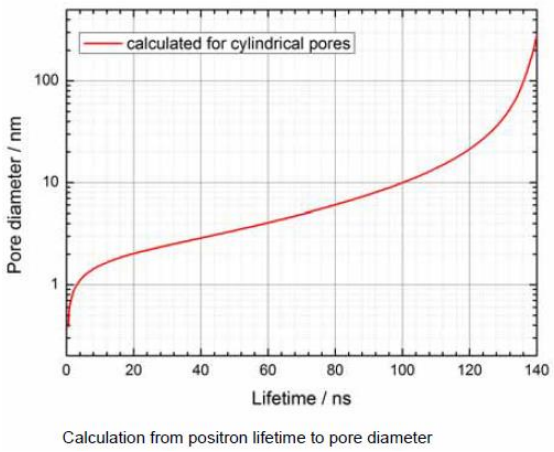

Fig. A3. Plot for calculation of pore diameter based on positron lifetime according to a shape-free model, based on the extended Tao Eldrup model [43].

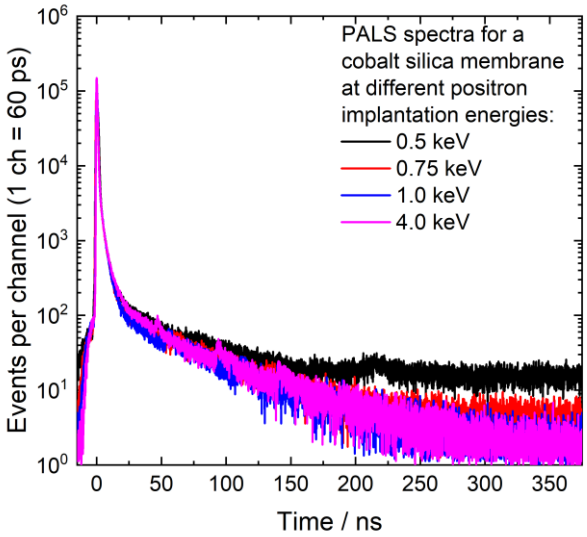

Fig. A4. Exemplary Positron Annihilation Lifetime spectra of a surfactant functionalised cobalt silica membrane (*x=1*) for different positron implantation energies.

Within the maximum entropy method, the entropy weight parameter *a* controls the competition between entropy solution and data constraints [48]. For a = 0, the solution is the pure least squares fitting result obtained by the standard PALS analysis using a multi-exponential decay approach. By

varying *a*, a series of solutions with different probabilities is obtained where usually the solution with the largest probability is chosen (Fig. A5).

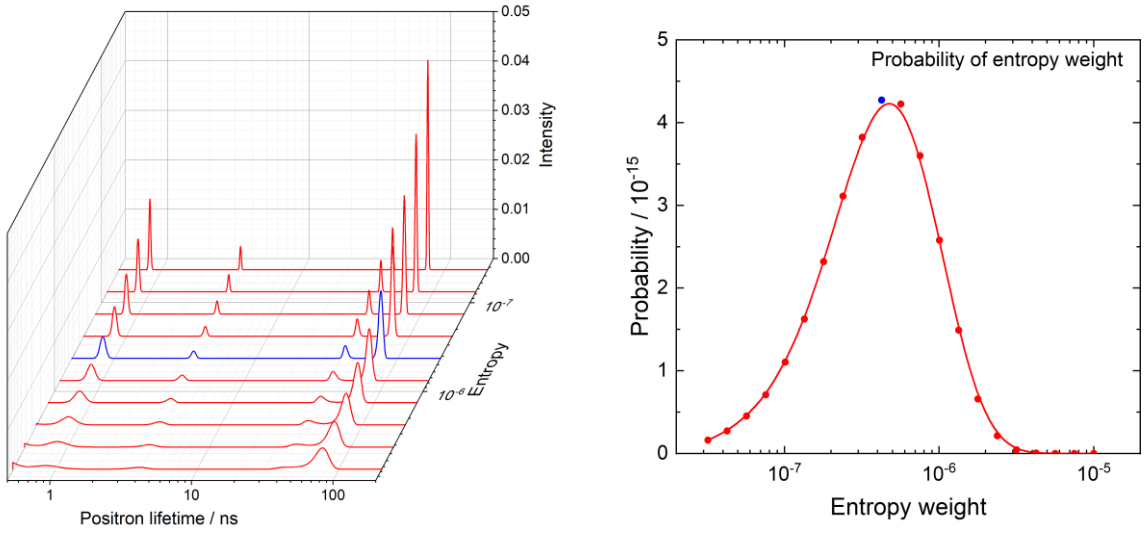

Fig. A5. Exemplary MELT analysis of a surfactant functionalised cobalt silica membrane recorded at positron energy of 6 keV (mean implantation depth 320 nm) with solutions for different entropies (left) and the probability for each entropy weight (right). The blue curve (left) and dot (right) are the chosen solutions with the maximum entropy.

References

[1] A.R. Smith, J. Klosek, A review of air separation technologies and their integration with energy conversion processes, Fuel Proc. Technol. 70 (2001) 115-134.

[2] M.A. Moreira, A.M. Ribeiro, A.F.P. Ferreira, A.E. Rodrigues, Cryogenic pressure temperature swing adsorption process for natural gas upgrade, Sep. Purif. Technol. 173 (2017) 339-356.

[3] S.K. Wirawan, D. Creaser, Multicomponent H_2/CO/CO_2 adsorption on BaZSM-5 zeolite, Sep. Purif. Technol. 52 (2006) 224-231.

[4] N.N. Linneen, R. Pfeffer, Y.S. Lin, CO_2 adsorption performance for amine grafted particulate silica aerogels, Chem. Eng. J. 254 (2014) 190-197.

[5] F.J. Tamajón, Estrella Álvarez, Fernando Cerdeira, Diego Gómez-Díaz, CO_2 absorption into N-methyldiethanolamine aqueous-organic solvents, Chem. Eng. J. 283 (2016) 1069-1080.

[6] Q. Ye, L. Zhu, X. Wang, Y. Lu, On the mechanisms of CO_2 absorption and desorption with phase transitional solvents, Int. J. Greenhouse Gas Cont. 56 (2017) 278-288.

[7] D. S. Sholl, R. P. Lively, Seven chemical reactions to change the world, Nature 532 (2006) 435–437.

[8] S. Smart, C.X.C. Lin, L. Ding, K. Thambimuthu, J.C. Diniz da Costa, Ceramic membranes for gas processing in coal gasification, Energy Environ. Sci. 3 (2010) 268–278.

[9] N.A. Al-Mufachi, N.V. Rees, R. Steinberger-Wilkens, Hydrogen selective membranes: A review of palladium-based dense metal membranes, Renewable Sustain. Energy Rev. 47 (2015) 540-551.

[10] N.W. Ockwig, T.M. Nenoff, Membranes for hydrogen separation, Chemical Rev. 107, 2007, 4078-4110.

[11] P. Bernardo, E. Drioli, G. Golemme, Membrane Gas Separation: A Review/State of the Art, Ind. Eng. Chem. Res. 48, 2009, 4638-4663.

[12] N. Moriyama, H. Nagasawa, M. Kanezashi, T. Tsuru, Selective water vapor permeation from steam/non-condensable gas mixtures via organosilica membranes at moderate-to-high temperatures, J. Membr. Sci. 589 (2019) 117254.

[13] C. Yacou, S. Smart, J. C. Diniz da Costa, Long term performance of a multi-tube cobalt oxide silica membrane at high temperatures for gas separation, Energy Environ. Sci. 5 (2012) 5820–5832.

[14] R. Igi, T. Yoshioka, Y.H. Ikuhara, Y. Iwamoto, T. Tsuru, Characterization of co-doped silica for improved hydrothermal stability and application to hydrogen separation membranes at high temperatures, J. Am. Ceram. Soc., 91 (2008) 2975-2981.

401 [15] S. Battersby, B. Ladewig, S. Liu, M.C. Duke, V. Rudolph, J.C. Diniz da Costa, Hydrothermal
402 stability of cobalt doped silica membranes in a water gas shift membrane reactor, Sep. Purif.
403 Technol. 66 (2009) 299–305.
404 [16] D. Uhlmann, S. Smart, J. C. Diniz da Costa, High Temperature Steam Investigation of Cobalt
405 Oxide Silica Membranes for Gas Separation, Sep. Purif. Technol. 76 (2010) 171–178.
406 [17] L. Liu, D.K. Wang, D.L. Martens, S. Smart, J.C. Diniz da Costa, Influence of the cobalt phase
407 sol-gel conditioning on the hydrothermal stability of cobalt doped silica membranes, J. Membr.
408 Sci. 475 (2015) 425–432.
409 [18] L. Liu, D.K. Wang, P. Kappen, D.L. Martens, S. Smart, J.C. Diniz da Costa, Hydrothermal
410 stability investigation of microporous silica containing long-range ordered cobalt oxide clusters
411 by XAS, Phys. Chem. Chem. Phys. 17 (2015) 19500-19506.
412 [19] M. Kanezashi, T. Fujita, M. Asaeda, Nickel-doped silica membranes for separation of helium
413 from organic gas mixtures, Sep. Sci. Technol., 40 (2005) 225-238.
414 [20] M. Kanezashi, M. Asaeda, Hydrogen permeation characteristics and stability of Ni-doped silica
415 membranes in steam at high temperature, J. Membr. Sci. 271 (2006) 86-93.
416 [21] Y.F. Gu, P. Hacarlioglu, S.T. Oyama, Hydrothermally stable silica-alumina composite
417 membranes for hydrogen separation, J. Membr. Sci., 310 (2008) 28-37.
418 [22] K. Yoshida, Y. Hirano, H. Fujii, T. Tsuru, Hydrothermal stability and performance of silica-
419 zirconia membranes for hydrogen separation in hydrothermal conditions, J. Chem. Eng. Jap. 34
420 (2001) 523-530.
421 [23] Y. Gu, S.T. Oyama, Permeation properties and hydrothermal stability of silica-titania membranes
422 supported on porous alumina substrates, J. Membr. Sci. 345 (2009) 267-275.
423 [24] V. Boffa, D.H.A. Blank, J.E. ten Elshof, Hydrothermal stability of microporous silica and niobia–
424 silica membranes, J. Membr. Sci. 319 (2008) 256-263.

425 [25] A. Darmawan, J. Motuzas, S. Smart, A. Julbe, J.C. Diniz da Costa, Binary Iron Cobalt Oxide
426 Silica Membrane for Gas Separation, J. Membr. Sci. 474(2015) 32–38.
427 [26] B. Ballinger, J. Motuzas, S. Smart, J.C. Diniz da Costa, Palladium Cobalt Binary Doping of
428 Molecular Sieving Silica Membranes, J. Membr. Sci. 451(2014)185–191
429 [27] B. Ballinger, J. Motuzas, S. Smart, J.C. Diniz da Costa, Redox effect on binary lanthanum cobalt
430 silica membranes with enhanced silicate formation, J. Membr. Sci. 489 (2015) 220–226.
431 [28] V Boffa, JE ten Elshof, AV Petukhov, DHA Blank, Microporous niobia–silica membrane with
432 very low CO_2 permeability, ChemSusChem 1 (2008) 437-443.
433 [29] G. Ji, S. Smart, S.K. Bhatia, J.C. Diniz da Costa, Pore connectivity effect by the reduction of
434 cobalt oxide silica membrane for gas permeation at high temperature, Sep. Purif. Technol. 154
435 (2015) 338–344.
436 [30] J.Y. Park, O. Levenspiel, The crackling core model for the reaction of solid particles, Chem. Eng.
437 Sci., 30 (1975) 1207-1214.
438 [31] G. Uhde, U. Hoffmann, Noncatalytic gas-solid reactions: modelling of simultaneous reaction and
439 formation of surface with a nonisothermal crackling core model, Chem. Eng. Sci., 52 (1997)
440 1045-1054.
441 [32] G. Olguin, C. Yacou, S. Smart, J.C. Diniz da Costa, Tailoring the oxidation state of cobalt
442 through halide functionality in sol-gel silica, Sci. Rep. 3 (2013) 2449 doi:10.1038/srep02449.
443 [33] R.M. de Vos, W.F. Maier, H. Verweij, Hydrophobic silica membranes for gas separation, J.
444 Membr. Sci. 158 (1999) 277-288.
445 [34] M.C. Duke, J.C. Diniz da Costa, D.D. Do, P.G. Gray, G.Q. Lu, Hydrothermally Robust
446 Molecular Sieve Silica for Wet Gas Separation, Adv. Funct. Mater. 16 (2006) 1215-1220.
447 [35] G. Olguin, C. Yacou, S. Smart, J.C. Diniz da Costa, Influence of surfactant alkyl length in
448 functionalizing sol-gel derived microporous cobalt oxide silica, RSC Adv. 4 (2014) 40181–
449 40187.

[36] S.K. Sharma, P. Maheshwari, D. Dutta, K. Sudarshan, P.K. Pujari, Modification of microstructure of the surface and the bulk in ion-irradiated membrane studied using positron annihilation spectroscopy, Rad. Phys. Chem. 79 (2010). 1115-1119.

[37] F. Constantin, C. Barna, P. Mereuta, Positron annihilation spectroscopy studies of proton exchange membranes used in fuel cells, Polymers for Advanced Technologies 26 (2015) 1528-1530.

[38] C.-C. Hu, K.-R. Lee, R.-C. Ruaan, Y.C.Jean, J.-Y. Lai, Gas separation properties in cyclic olefin copolymer membrane studied by positron annihilation, sorption, and gas permeation J. Membr. Sci. 274 (2006), 192-199.

[39] X. Ma, H. Wang, H. Wang, J. O'Brien-Abraham, Y.S.Li, Pore structure characterization of supported polycrystalline zeolite membranes by positron annihilation spectroscopy, J. Membr. Sci. 477 (2015) 41-48.

[40] C.-Y. Tsai, S.-Y. Tam, Y. Lu, C.J. Brinker, Dual-layer asymmetric microporous silica membranes, J. Membr. Sci. 169 (2000) 255-268.

[41] H. Gharibi, B.M. Razavizadeh, A.A. Rafati, Electrochemical studies associated with the micellization of dodecyltrimethyl ammonium bromide (DOTAB) in aqueous solutions of ethanol and l-propanol, Coll. Surf. A –Physicochem. Eng. Asp. 136 (1998) 123-132.

[42] J.B. Huang, M. Mao, B.Y. Zhu, The surface physico-chemical properties of surfactants in ethanol-water mixtures, Coll. Surf. A –Physicochem. Eng. Asp. 155 (1999) 339-348.

[43] E. Fuguet, C. Ràfols, M. Rosés, E. Bosch, Critical micelle concentration of surfactants in aqueous buffered and unbuffered systems, Analytica Chim. Acta 548 (2005) 95-100.

[44] A. Wagner, W. Anwand, A.G. Attallah, G. Dornberg, M. Elsayed, D. Enke, A.E.M. Hussein, R. Krause-Rehberg, M.O. Liedke, K. Potzger, T.T. Trinh, Positron annihilation lifetime spectroscopy at a superconducting electron Accelerator, J. Phys.: Conf. Ser. 791 (2017) 012004.

[45] A. Wagner, M. Butterling, M.O. Liedke, K. Potzger, R. Krause-Rehberg, Positron annihilation lifetime and Doppler broadening spectroscopy at the ELBE facility, AIP Conf. Proc. 1970 (2018) 040003.

[46] M.J. Puska, R. M. Nieminen, Theory of positrons in solids and on solid surfaces, Rev. Modern Phys. 66 (1994) 841–97.

[47] K. Wada, T. Hyodo, A simple shape-free model for pore-size estimation with positron annihilation lifetime spectroscopy, J. Phys.: Conf. Ser. 443 (2013) 012003.

[48] A. Shukla, M. Peter, L. Hoffmann, Analysis of positron lifetime spectra using quantified maximum entropy and a general linear filter, Nucl. Instrum. Methods Phys. Res. A 335 (1993) 310-317.

[49] M.C. Duke, S.J. Pas, A.J. Hill, Y.S. Lin, J.C. Diniz da Costa, Exposing the molecular sieving architecture of amorphous silica using positron annihilation spectroscopy, Adv. Funct. Mater. 18 (2008) 3818-3826.

[50] D. Uhlmann, S. Liu, B. P. Ladewig, J. C. Diniz da Costa, Cobalt-doped silica membranes for gas separation, J. Membr. Sci. 326 (2009) 316–321.

[51] R.M. de Vos, H. Verweij, Improved performance of silica membranes for gas separation, J. Membr. Sci. 143 (1998) 37-51.

[52] J.C. Diniz da Costa, G.Q. Lu, V. Rudolph, Y.S. Lin, Novel molecular sieve silica (MSS) membranes: characterisation and permeation of single-step and two-step sol–gel membranes, J. Membr. Sci. 198 (2002) 9-21.

[53] R.S.A. de Lange, K. Keizer, A.J. Burggraaf, Analysis and theory of gas transport in microporous sol-gel derived ceramic membranes, J. Membr. Sci. 104 (1995) 81-100.

[54] R. M. Barrer, Porous Crystal Membranes, J. Chem. Soc. Faraday Trans. 86 (1990)1123-1130.

[55] W.J. Bakker, L.J.P. van den Broeke, F. Kapteijn, J. A. Moulijn, Temperature dependence of one-component permeation through a silicalite-1 membrane, AIChE J. 43 (1997) 2203-2214.

[56] C. J. Brinker, G. W. Scherer, Sol Gel Science: the physics and chemistry of the sol gel processing, (1990) Academic Press, San Diego, USA.

[57] C.J. Brinker, A.J. Hurd, K.J. Ward, Fundamentals of sol-gel thin-film formation in: Ultrastructure Processing of Advanced Ceramics, eds J. D. Mackenzie, D. R. Ulrich, Wiley, New York (1988) 223-253.

[58] D.L. Meixner, P.N. Dyer, Characterisation of the transport properties of microporous inorganic membranes, J. Membr. Sci. 140 (1998) 81-95.